

Real-time dynamics of spin-dependent transport through a double-quantum-dot Aharonov-Bohm interferometer with spin-orbit interaction

Matisse Wei-Yuan Tu,¹ Amnon Aharony,^{2,3,*} Wei-Min Zhang,^{1,†} and Ora Entin-Wohlman^{2,3}

¹*Department of Physics, National Cheng Kung University, Tainan 70101, Taiwan*

²*Physics Department, Ben Gurion University, Beer Sheva 84105, Israel*

³*Raymond and Beverly Sackler School of Physics and Astronomy, Tel Aviv University, Tel Aviv 69978, Israel*

The spin-resolved non-equilibrium real-time electron transport through a double-quantum-dot (DQD) Aharonov-Bohm (AB) interferometer with spin-orbit interaction (SOI) is explored, using the solution to an exact master equation. The SOI and AB interference in the real-time dynamics of spin transport is expressed by effective magnetic fluxes. Analytical formulae for the time-dependent currents, for initially unpolarized spins, are presented. In many cases, there appear spin currents in the electrodes, for which the spins in each electrode are polarized along characteristic directions, pre-determined by the SOI parameters and by the geometry of the system. Special choices of the system parameters yield steady-state currents in which the spins are fully polarized along these characteristic directions. The time required to reach this steady state depends on the couplings of the DQD to the leads. The magnitudes of the currents depend strongly on the SOI-induced effective fluxes. Without the magnetic flux, the spin-polarized current cannot be sustained to the steady states, due to the phase rigidity for this system. For a non-degenerate DQD, transient spin transport can be produced by the sole effects of SOI. We also show that one can extract the spin-resolved currents from measurements of the total charge current.

PACS numbers: 72.25.Dc,75.70.Tj,72.25.Rb,85.35.-p

I. INTRODUCTION

Electron interference in nanoscale quantum transport systems has long been a focus of intensive research. Of particular interest are the Aharonov-Bohm (AB)¹ and the Aharonov-Cahser (AC)² effects, associated with the two fundamental degrees of freedom of an electron, namely, the charge and the spin. By tuning externally applied fields, one is able to modulate these interference effects and thus affect the quantum transport properties. Interesting results of coherence modulation have been found from the studies of stationary properties of these interferometer systems. Dynamical responses of interference devices to periodically applied driving fields have also caught attention, due to their potentials in applications. In addition, there is a rising interest in the real time dynamics of the charge and spin transport in such devices. This is relevant to temporal operations of quantum devices and also to the understanding of various physical processes. More and more attention is thus paid to the transient evolution of coherent electron transport. Naturally, the effects of interference on the transient dynamics of non-equilibrium transport is an important issue. In this work, we study the dynamical evolution of electron transport through a double-quantum-dot (DQD) Aharonov-Bohm interferometer with spin-orbit interaction (SOI).

Coherence of the electron's orbital motion underlies the conductance oscillation in the applied magnetic flux, enclosed by low-dimensional electronic systems.³⁻⁶ Studies of AB oscillations in AB interferometers with quantum dots have been realized in experiments.⁷⁻¹⁰ Analogous to this AB oscillation, systems where the spin-orbit interaction is present exhibit conductance oscillations

in the SOI strength, known as AC oscillations.¹¹ Signatures of the AC effects have also been observed in experiments.¹²⁻¹⁴ Besides interference effects in ring-shaped structures, SOI in nanoelectronic systems in general is known to have an important role in spintronics.¹⁵ An important task in spintronics is to generate spin-polarized currents.

An early initiative in spintronics is the proposal of the spin-field-effect transistor by Datta and Das, that combined the SOI with ferromagnets.¹⁶ Optical spin injection into ferromagnets for generating spin-polarized currents was experimentally implemented.¹⁷ Electrical spin injection from ferromagnets to semiconductors was also realized.¹⁸ Spin-polarized currents can also be generated using magnetic tunnel junctions.¹⁹⁻²² Impedance mismatch between ferromagnets and semiconductors hinders efficient operation of spin injection,²³ whose solution requires special techniques.²⁴ Generating spin-polarized currents without the use of ferromagnets, but with tunable SOI, is an alternative option. There are two kinds of SOI in mesoscopic electronic structures receiving special attentions, namely, the Dresselhaus SOI²⁵ and Rashba SOI.²⁶ The former is a property of crystal structures that lack inversion symmetry in their unit cells. The latter, induced by the asymmetry in externally applied confinement potential, can be controlled by tuning this external electric field. The tunability of Rashba SOI strength has been demonstrated experimentally,^{12,13,27,28} making the utilisation of SOI for generating spin-polarized current viable.

The simplest system that exhibits both the AB and the AC interference phenomena is a single loop. The loop is threaded by a magnetic flux and an electron can flip its spins as it tunnels along the loop. By at-

taching current leads to the loop, transport properties can be investigated. Spin interference effects on the electron transport through this kind of structures have been widely investigated. Many papers consider generating spin-polarized currents in such systems. These cover the modulation of conductance in one-dimensional and also two-dimensional circular rings,^{29–32} and the effects of the coupling between the DQD and the leads on spin-dependent transport.^{33,34} Alternative system geometries, like polygons, have also been studied.^{35,36} Instead of using just two leads, results from attaching three leads to the ring, mimicking a Stern-Gerlach experiment, have also been reported.^{37,38} Diamond-like loops have been found to exhibit fully polarized spin currents.^{39–41} SOI in parallel DQD with inter-dot tunnel couplings have been considered.^{42–45} Though interference is mostly effective at low temperatures, results from high temperature single-channel ring are also analyzed.⁴⁶ Furthermore, electron-electron interactions are studied in rings with SOI.^{47,48} Besides focusing on the time-independent aspect, time-periodical varying SOI has attracted attention,^{49,50} as spin pumping devices.

Apart from this, much effort has been poured into the research of time-dependent electron transport through nanojunctions. Experimentally, time-resolved transport measurements have been implemented.^{51–53} Theoretically, a multitude of approaches, focusing on many different aspects, has been devoted to understand the real-time electron dynamics in quantum transport.^{54–65} Real-time dynamics concerning spin-resolved currents have also been reported. By solving the time-dependent Schrödinger equation, the spin-resolved time evolution of the electron wave function in a ring with oscillating SOI has been analyzed.⁵⁰ Time evolution of electron wave functions with different spins has also been considered in quantum well structures.⁶⁶ Applying a method for propagating Green functions in time,⁵⁸ transient spin-dependent currents through a single-level dot, without a loop structure, has been studied.⁶⁷ In our previous work,^{68,69} we have investigated the transient electron dynamics in a spinless DQD AB interferometer, using a non-equilibrium formalism.^{63,64} An earlier work had studied the steady states of a similar system with spins and SOI.⁴¹ By the use of scattering theory, it has been proved that such system can function as a spin filter under appropriate conditions.⁴¹ Therefore we are interested in including spins and SOI in such a DQD AB interferometer and study the transient dynamics of spin-dependent transport.

The target system in this work is illustrated in Fig. 1. We apply our previously developed approach^{63,64} for monitoring electron dynamics and real-time transport in nano-electronic systems to the present case. We adopt the prescription for spin transformation along electron tunneling paths given in Ref. [70], and used in [41]. Fully spin-polarized currents have been obtained in the steady-state limit using the spin filter conditions given in Ref. [41] (see sections III and IV). The spin-independent real-

time total current is found to be the sum of two currents. Each of them is the current for the same spinless system, but with the flux replaced by an effective flux, combining the AB phase and the SOI-induced phase (see discussions in section III). This time-dependent result is consistent with the universal behavior in rings with SOI pointed out in Ref. [71]. In particular, we present the processes of the growth of the spin polarization in the currents, starting from totally unpolarized initial states of the system. We discuss how different parameters of the system affect these processes and the consequent time scales for steady-state spin polarization to appear. We analyze the transport of spins in the context of the interplay between the SOI and the AB effects. Since it is easier to measure spin-independent quantities in experiments, we also discuss how to extract the spin-polarized currents from spin-independent transport quantities in our target system.

Our main results are as follows. With the interferometer being initially unpolarized, the intrinsic mechanisms of SOI cause the current in electrode α to develop polarization only in some special direction, $\hat{\mathbf{n}}_\alpha$, for all time t , where $\alpha = L, R$ represent the left and right leads. These special directions $\hat{\mathbf{n}}_L$ and $\hat{\mathbf{n}}_R$ are characteristic of these electrodes, and they are purely determined by the SOI parameters. In general, the currents in these two leads are polarized along different directions. We denote the current in lead α carrying electrons with spins along the characteristic direction, $\hat{\mathbf{n}}_\alpha$, by $I_{\alpha\hat{\mathbf{n}}_\alpha;\pm}(t)$, where $+$ and $-$ stand for spin-up and spin-down. We find that these currents can be identified with those for the same spinless DQD AB interferometers, but with the threading flux replaced by the effective fluxes $\varphi_\pm = \phi \pm \psi_{\text{so}}$. The latter is denoted by $I_\alpha^0(\varphi_\pm, t)$ and we have $I_{\alpha\hat{\mathbf{n}}_\alpha;\pm}(t) = I_\alpha^0(\varphi_\pm, t)$. Here ϕ is the applied magnetic flux and ψ_{so} is the phase purely induced by SOI. The effective fluxes, the on-site energies of the DQD and its couplings to the electrodes together fix the configurations of the underlying spinless AB interferometers that in turn determine the spin polarizations of the currents. When these parameters satisfy the conditions for achieving fully spin-polarized currents, in which φ_- is required to be an odd integer multiple of π , the two electrodes of the spinless interferometer with the effective flux φ_- become effectively disconnected. Otherwise for φ_\pm being away from odd integers of π , the two electrodes remain connected. Consequently in case fully spin-polarized currents are to arise, the processes of the spin-down currents decay to zero separately in the two electrodes. At the same time, the spin-up currents are correlated between the two sides. The couplings between the DQD and the electrodes largely determine the times to reach stable polarization in the currents. The effective fluxes, which control the interference between the upper and the lower paths of the corresponding spinless interferometers, modulate the magnitudes of the polarized currents. The spin current in lead α , defined as the time derivative of the total spin in that lead, is found to be proportional to $I_\alpha^0(\varphi_+, t) - I_\alpha^0(\varphi_-, t)$. Since the un-

derlying spinless interferometer is a two-terminal system, the steady-state currents are subject to phase rigidity, namely, $I_\alpha^0(\varphi_\pm, t \rightarrow \infty) = I_\alpha^0(-\varphi_\pm, t \rightarrow \infty)$, see Ref. [69] and references therein. Therefore, the currents can remain polarized to the steady-state limit, $t \rightarrow \infty$, only if $\varphi_+ \neq -\varphi_-$. For $\phi = 0$, one has $\varphi_\pm = \pm\psi_{so}$ and thus the magnetic flux is essential for stable spin-polarized transport.

The paper is organized as follows. In section II, we summarize our general methodology with both spin and charge degrees of freedom. We introduce our model with a description of its SOI features in section III A. In section III B, we utilize the characteristic spinors of the SOI-induced unitary spin rotations, to show that the Hamiltonian of the target system can be decomposed into two commuting components, one for spin-up states and the other for spin-down states. Based on such decomposition, in section III C, we deduce the aforementioned main results about spin polarization properties directly on the level of the Hamiltonian. Obtaining fully spin-polarized currents using the conditions given in Ref. [41] is also shown. In section III D, the methodology summarized in section II is applied to the target system of a DQD AB interferometer with the SOI introduced in section III A. Analytical formulae for the currents, with an emphasis on the role of spin-dependence, are obtained. These expressions in terms of Green functions supplement the analysis in section III C. To demonstrate the functioning of these physical factors behind spin-polarized transport with concrete examples, we take the commonly assumed wide-band limit for specific calculations. In section IV, we first take the steady-state limit to reassure the reproduction of fully spin-polarized currents. We also analyze the situation when the setup of the system deviates from these conditions. This is followed by instructions for extracting the spin-polarized transmission from the spin-independent total transmission (which is much more accessible experimentally). Section V is divided into three parts. In section V A, we focus on the dynamics of getting fully spin-polarized currents. In section V B, general parameters are explored to understand the transport of spins under the influence of charge and spin interferences. In addition, utilizing the results from section IV, we also devise similar ideas for extracting the spin-polarized currents from the spin-independent total charge currents in section V C. Conclusions and a summary are given in section VI.

II. SUMMARY OF THE BASIC FORMALISM USED FOR OPEN SYSTEM NANO-TRANSPORT

Here we briefly present the main results of our previously developed open quantum system prescription for non-equilibrium electron transport dynamics through nano-electronic structures. In order to consider spin-dependent dynamics, here we label both the charge and the spin degrees of freedom explicitly. We also assume

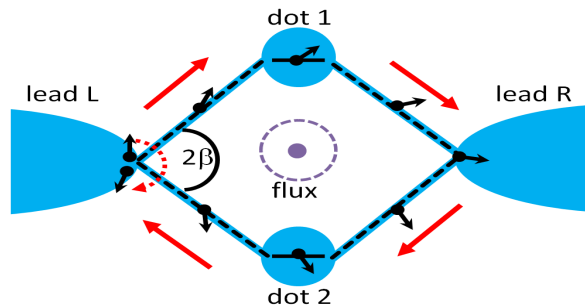


FIG. 1: (color online) A sketch of a DQD AB interferometer with SOI. Each of the two dots contains one charge state with a spin. The dots are placed in parallel between two leads L and R . A magnetic flux threads through the loop formed by the two dots and the two leads. The electron spin rotates as it tunnels along the loop, due to the SOI. The hopping energies along the upper branch (through dot 1) and along the lower branch (through dot 2) are symmetric. The angle between the two paths is 2β .

that electron reservoirs are free from SOI. The general Hamiltonian under consideration is then given by

$$\mathcal{H} = \mathcal{H}_S + \mathcal{H}_E + \mathcal{H}_T \quad (1)$$

where

$$\mathcal{H}_S = \sum_{ij, \sigma\sigma'} E_{i\sigma, j\sigma'} a_{i\sigma}^\dagger a_{j\sigma'} \quad (2)$$

is the Hamiltonian of the central area with i, j labeling orbital states and σ, σ' denoting the spins,

$$\mathcal{H}_E = \sum_{\alpha k\sigma} \epsilon_{\alpha k} c_{\alpha k\sigma}^\dagger c_{\alpha k\sigma} \quad (3)$$

is the Hamiltonian for electron reservoirs with α labeling the leads and $k\sigma$ denoting the states in the leads with orbital quantum number k and spin σ , and

$$\mathcal{H}_T = \sum_{i\alpha k} \sum_{\sigma\sigma'} [V_{i\sigma, \alpha k\sigma'} a_{i\sigma}^\dagger c_{\alpha k\sigma'} + \text{h.c.}] \quad (4)$$

describes the tunneling between the central system and the leads. Here $a_{i\sigma}^\dagger$ ($a_{i\sigma}$) and $c_{\alpha k\sigma}^\dagger$ ($c_{\alpha k\sigma}$) are the electron creation (annihilation) operators for electronic levels $i\sigma$ and $k\sigma$ in the scattering area and in the lead α , respectively. In all the above equations, the spins are quantized along an arbitrary direction.

The central system is open to the electron reservoirs. Its non-equilibrium dynamics is described by the reduced density matrix $\rho(t)$, which is obtained by tracing over the states of the leads,

$$\rho(t) = \text{tr}_E \rho_{\text{tot}}(t) = \text{tr}_E [e^{-i\mathcal{H}(t-t_0)} \rho_{\text{tot}}(t_0) e^{i\mathcal{H}(t-t_0)}], \quad (5)$$

where $\rho_{\text{tot}}(t)$ is the total density matrix of the central system plus the electron reservoirs. Electronic occupations and coherence on the electronic states of the central system can be found from $\rho(t)$. The electronic transport

through the central system is characterized by the currents flowing from the leads into the central scattering region, defined by

$$I_{\alpha\sigma}(t) = -\frac{d}{dt} \sum_{\mathbf{k} \in \alpha} \text{tr}_{\text{tot}} [c_{\alpha\mathbf{k}\sigma}^\dagger c_{\alpha\mathbf{k}\sigma} \rho_{\text{tot}}(t)], \quad (6)$$

as the current flowing to lead α with spin σ . This can be further decomposed into separate contributions through each level in the central system:

$$I_{\alpha\sigma}(t) = \sum_{i\sigma'} I_{i\sigma',\alpha\sigma}(t), \quad (7a)$$

$$I_{i\sigma',\alpha\sigma}(t) = -i \sum_{\mathbf{k} \in \alpha} \text{tr}_{\text{tot}} [V_{i\sigma',\alpha\mathbf{k}\sigma} a_{i\sigma'}^\dagger c_{\alpha\mathbf{k}\sigma} \rho_{\text{tot}}(t) - \text{h.c.}]. \quad (7b)$$

In Eqs. (5) and (7b), tr_E and tr_{tot} denote the traces over the states of the leads and the total system, respectively. Throughout the paper, we use units in which $\hbar = e = 1$.

As usual, we assume⁷² that the central system is initially decoupled from the leads, and the leads are initially at thermal equilibrium with the chemical potential $\mu_{\alpha\sigma}$ and the temperature $T_{\alpha\sigma}$ for electron with spin σ in lead α , whose Fermi distribution function is given by,

$$f_{\alpha\sigma}(\omega) = 1/[e^{(\omega - \mu_{\alpha\sigma})/k_B T_{\alpha\sigma}} + 1], \quad (8)$$

where k_B is the Boltzmann constant. Then the exact equations for the time evolution of the reduced density matrix and the transient currents are^{63,64}

$$\frac{d}{dt} \rho(t) = -i[\mathcal{H}_S, \rho(t)] + \sum_{i\sigma, \alpha\sigma'} [\mathcal{L}_{i\sigma, \alpha\sigma'}^+(t) + \mathcal{L}_{i\sigma, \alpha\sigma'}^-(t)] \rho(t), \quad (9a)$$

$$I_{i\sigma, \alpha\sigma'}(t) = \text{tr}_S [\mathcal{L}_{i\sigma, \alpha\sigma'}^+(t) \rho(t)] = -\text{tr}_S [\mathcal{L}_{i\sigma, \alpha\sigma'}^-(t) \rho(t)], \quad (9b)$$

where the superoperators $\mathcal{L}_{i\sigma, \alpha\sigma'}^\pm(t)$ are expressed explicitly by

$$\begin{aligned} & \mathcal{L}_{i\sigma, \alpha\sigma'}^+(t) \rho(t) \\ &= - \sum_{j\sigma''} \left\{ [\boldsymbol{\lambda}(t)_{\alpha\sigma'}]_{i\sigma, j\sigma''} [a_{i\sigma}^\dagger a_{j\sigma''} \rho(t) + a_{i\sigma}^\dagger \rho(t) a_{j\sigma''}] \right. \\ & \quad \left. + [\boldsymbol{\kappa}(t)_{\alpha\sigma'}]_{i\sigma, j\sigma''} a_{i\sigma}^\dagger a_{j\sigma''} \rho(t) + \text{h.c.} \right\}, \\ & \mathcal{L}_{i\sigma, \alpha\sigma'}^-(t) \rho(t) \\ &= \sum_{j\sigma''} \left\{ [\boldsymbol{\lambda}(t)_{\alpha\sigma'}]_{i\sigma, j\sigma''} [a_{j\sigma''} \rho(t) a_{i\sigma}^\dagger + \rho(t) a_{j\sigma''} a_{i\sigma}^\dagger] \right. \\ & \quad \left. + [\boldsymbol{\kappa}(t)_{\alpha\sigma'}]_{i\sigma, j\sigma''} a_{j\sigma''} \rho(t) a_{i\sigma}^\dagger + \text{h.c.} \right\}, \end{aligned} \quad (10)$$

and tr_S is the trace over the states in the central system. The first term on the right hand side of Eq. (9a) is the Liouville operator of the central system. The second

and the third terms, expressed in terms of the superoperators, are non-unitary. The non-unitarity is induced by electronic dissipation and fluctuation processes due to the couplings of the central system to the electronic reservoirs. The transient transport current is determined from the non-unitary dynamics, as shown by Eq. (9b). Equations (9) and (10) form the basis of the non-equilibrium description of quantum coherence and quantum transport in mesoscopic systems.

The time-dependent dissipation and fluctuation coefficients in Eqs. (10), $\boldsymbol{\kappa}_{\alpha\sigma'}(t)$ and $\boldsymbol{\lambda}_{\alpha\sigma'}(t)$, are explicitly determined by the non-equilibrium retarded and correlation Green functions of the central system, denoted here by $\mathbf{u}(t)$ and $\mathbf{v}(t)$,⁶⁴ via the relations

$$\boldsymbol{\kappa}_{\alpha\sigma'}(t) = \int_{t_0}^t d\tau \mathbf{g}_{\alpha\sigma'}(t, \tau) \mathbf{u}(\tau) \mathbf{u}^{-1}(t), \quad (11a)$$

$$\begin{aligned} \boldsymbol{\lambda}_{\alpha\sigma'}(t) &= \int_{t_0}^t d\tau \{ \mathbf{g}_{\alpha\sigma'}(t, \tau) \mathbf{v}(\tau) - \tilde{\mathbf{g}}_{\alpha\sigma'}(t, \tau) \bar{\mathbf{u}}(\tau) \} \\ &\quad - \boldsymbol{\kappa}_{\alpha\sigma'}(t) \mathbf{v}(t). \end{aligned} \quad (11b)$$

The self-energies due to the coupling to the leads are given by

$$\begin{aligned} \mathbf{g}_{\alpha\sigma}(\tau) &= \int \frac{d\omega}{2\pi} \boldsymbol{\Gamma}^{\alpha\sigma}(\omega) e^{-i\omega\tau}, \\ \tilde{\mathbf{g}}_{\alpha\sigma}(\tau) &= \int \frac{d\omega}{2\pi} f_{\alpha\sigma}(\omega) \boldsymbol{\Gamma}^{\alpha\sigma}(\omega) e^{-i\omega\tau}, \end{aligned} \quad (12a)$$

where the level-broadening function from coupling to electronic states of spin σ in lead α is

$$[\boldsymbol{\Gamma}^{\alpha\sigma}(\omega)]_{i\sigma', j\sigma''} = 2\pi \sum_{\mathbf{k} \in \alpha} V_{i\sigma', \alpha\mathbf{k}\sigma} V_{j\sigma'', \alpha\mathbf{k}\sigma}^* \delta(\omega - \epsilon_{\alpha\mathbf{k}}). \quad (12b)$$

The non-equilibrium retarded and correlation Green functions of the central system obey the following dissipation-fluctuation integro-differential equations of motion,

$$\frac{d}{d\tau} \mathbf{u}(\tau) + i\mathbf{E} \mathbf{u}(\tau) + \int_{t_0}^{\tau} d\tau' \mathbf{g}(\tau - \tau') \mathbf{u}(\tau') = 0, \quad (13a)$$

$$\begin{aligned} \frac{d}{d\tau} \mathbf{v}(\tau) + i\mathbf{E} \mathbf{v}(\tau) + \int_{t_0}^{\tau} d\tau' \mathbf{g}(\tau - \tau') \mathbf{v}(\tau') \\ = \int_{t_0}^t d\tau' \tilde{\mathbf{g}}(\tau - \tau') \bar{\mathbf{u}}(\tau'), \end{aligned} \quad (13b)$$

subjected to the conditions $\mathbf{u}(t_0) = I$, $\mathbf{v}(t_0) = 0$ with $t_0 \leq \tau \leq t$, and $\bar{\mathbf{u}}(\tau) = \mathbf{u}^\dagger(t - \tau + t_0)$ is the advanced Green function. Here \mathbf{E} is the energy matrix of the central system while

$$\mathbf{g}(\tau - \tau') = \sum_{\alpha\sigma} \mathbf{g}_{\alpha\sigma}(\tau - \tau'), \quad (14a)$$

$$\tilde{\mathbf{g}}(\tau - \tau') = \sum_{\alpha\sigma} \tilde{\mathbf{g}}_{\alpha\sigma}(\tau - \tau'), \quad (14b)$$

are the tunneling induced self-energies.

The correlation Green function $\mathbf{v}(t)$, Eq. (13b), has a general solution in terms of the retarded Green function $\mathbf{u}(\tau)$,

$$\mathbf{v}(\tau) = \int_{t_0}^{\tau} d\tau_1 \int_{t_0}^{\tau_1} d\tau_2 \mathbf{u}(\tau - \tau_1 + t_0) \tilde{\mathbf{g}}(\tau_1 - \tau_2) \bar{\mathbf{u}}(\tau_2). \quad (15)$$

From the master equation, Eq. (9a), it is easy to find the single-particle reduced density matrix in terms of $\mathbf{u}(t)$ and $\mathbf{v}(t)$:

$$[\boldsymbol{\rho}^{(1)}(t)]_{i\sigma, j\sigma'} \equiv \text{tr}[a_{j\sigma'}^\dagger a_{i\sigma} \boldsymbol{\rho}(t)], \quad (16a)$$

$$\boldsymbol{\rho}^{(1)}(t) = \mathbf{u}(t) \boldsymbol{\rho}^{(1)}(t_0) \mathbf{u}^\dagger(t) + \mathbf{v}(t), \quad (16b)$$

where $\boldsymbol{\rho}^{(1)}(t_0)$ is the initial single-particle reduced density matrix of the central system. The currents contributed by each level in the central system with orbital index i and spin σ to the current on lead α with spin σ' , Eq. (9b), can then be explicitly expressed as⁶⁴

$$\begin{aligned} I_{i\sigma, \alpha\sigma'}(t) = & \\ & - 2\text{Re} \int_{t_0}^t d\tau \{ \mathbf{g}_{\alpha\sigma'}(t - \tau) \mathbf{v}(\tau) - \tilde{\mathbf{g}}_{\alpha\sigma'}(t - \tau) \bar{\mathbf{u}}(\tau) \\ & + \mathbf{g}_{\alpha\sigma'}(t - \tau) \mathbf{u}(\tau) \boldsymbol{\rho}^{(1)}(t_0) \bar{\mathbf{u}}^\dagger(t) \}_{i\sigma, i\sigma'}. \end{aligned} \quad (17)$$

Summing over contributions from each of the single-particle states in the central system, the current for spin σ' in lead α is

$$\begin{aligned} I_{\alpha\sigma'}(t) = & \\ & - 2\text{TrRe} \int_{t_0}^t d\tau \{ \mathbf{g}_{\alpha\sigma'}(t - \tau) \mathbf{v}(\tau) - \tilde{\mathbf{g}}_{\alpha\sigma'}(t - \tau) \bar{\mathbf{u}}(\tau) \\ & + \mathbf{g}_{\alpha\sigma'}(t - \tau) \mathbf{u}(\tau) \boldsymbol{\rho}^{(1)}(t_0) \bar{\mathbf{u}}^\dagger(t) \}. \end{aligned} \quad (18)$$

This expression is consistent with the result obtained from the Keldysh Green function technique⁷³ (see the explicit derivation given in Ref. [64]).

For investigating the process of electron injection and the following dynamics of the current, we assume that initially the central area contains no excess electrons, namely, $\boldsymbol{\rho}^{(1)}(t_0) = 0$. In this case, the current formula, Eq. (18), is simplified to

$$\begin{aligned} I_{i\sigma, \alpha\sigma'}(t) = & \\ & 2\text{Re} \int_{t_0}^t d\tau \{ \tilde{\mathbf{g}}_{\alpha\sigma'}(t - \tau) \bar{\mathbf{u}}(\tau) - \mathbf{g}_{\alpha\sigma'}(t - \tau) \mathbf{v}(\tau) \}_{i\sigma, i\sigma'}, \end{aligned} \quad (19)$$

and consequently

$$\begin{aligned} I_{\alpha\sigma}(t) = & \\ & 2\text{ReTr} \int_{t_0}^t d\tau \{ \tilde{\mathbf{g}}_{\alpha\sigma}(t - \tau) \bar{\mathbf{u}}(\tau) - \mathbf{g}_{\alpha\sigma}(t - \tau) \mathbf{v}(\tau) \}. \end{aligned} \quad (20)$$

By specifying the level-broadening function, Eq. (12b), and therefore the self-energies, Eq. (12a), one can substitute them into Eqs. (13a, 13b) for solving the Green

functions in the time domain. The real time currents for the initially depleted central region can then be found by substituting these Green functions and self-energies into Eq. (20).

III. REAL-TIME TRANSPORT THROUGH A DQD AB INTERFEROMETER WITH SOI

A. The model

The DQD interferometer which we consider here is schematically presented in Fig. 1. It is composed of three parts, the DQD, the two electron reservoirs on the left and on the right and the tunneling between the DQD and the electrodes. The electron reservoirs are free from SOI. The total Hamiltonian is then generally given by Eq. (1).

Here we focus only on SOI and ignore Zeeman splitting. Explicitly, the central system Hamiltonian, Eq. (2), is specified to,

$$\mathcal{H}_S = \sum_{\sigma} \sum_{i=1}^2 E_i a_{i\sigma}^\dagger a_{i\sigma}. \quad (21)$$

The DQD system is spin-degenerate with E_i 's being the on-site energies for the single-level charge state in dot i . The operator $a_{i\sigma}^\dagger$ ($a_{i\sigma}$) creates (annihilates) an electron in the single-level charge state i with spin σ . The Hamiltonian for SOI-free electron reservoirs, \mathcal{H}_E , is described by Eq. (3). In the present case we have only two leads, $\alpha = L, R$. Due to the SOI, flipping of the spin can occur when an electron tunnels forth and back between the DQD and the leads. The tunneling Hamiltonian, Eq. (4), is then specified by the tunneling amplitudes,

$$V_{i\sigma, \alpha\mathbf{k}\sigma'} = V_{i\alpha\mathbf{k}} \langle \sigma | U^{i\alpha} | \sigma' \rangle, \quad (22)$$

which contain two separate parts. The spatial part $V_{i\alpha\mathbf{k}} = \bar{V}_{i\alpha\mathbf{k}} e^{i\phi_{i\alpha}}$ embeds the AB phase. The phases are constrained by the relation

$$\phi = \phi_L - \phi_R, \quad (23)$$

with $\phi_\alpha = \phi_{1\alpha} - \phi_{2\alpha}$ for $\alpha = L, R$. Here $\phi = \Phi/\Phi_0$, where Φ is the applied magnetic flux and Φ_0 is the flux quantum. The accompanying spin rotation due to the SOI is a unitary operation $U^{i\alpha}$, determined by the underlying bonding geometry.

Specifically, if the system lies on the x - y plane, then these rotations are^{41,70}

$$U^{i\alpha} = \exp(i\mathbf{K}^{i\alpha} \cdot \boldsymbol{\sigma}) \quad (24a)$$

where $\boldsymbol{\sigma} = \sigma_x \hat{\mathbf{x}} + \sigma_y \hat{\mathbf{y}} + \sigma_z \hat{\mathbf{z}}$, is the vector of Pauli matrices and

$$\begin{aligned} \mathbf{K}^{i\alpha} = & (\alpha_R \hat{\mathbf{g}}^{i\alpha} \cdot \hat{\mathbf{y}} + \alpha_D \hat{\mathbf{g}}^{i\alpha} \cdot \hat{\mathbf{x}}) \hat{\mathbf{x}} \\ & - (\alpha_R \hat{\mathbf{g}}^{i\alpha} \cdot \hat{\mathbf{x}} + \alpha_D \hat{\mathbf{g}}^{i\alpha} \cdot \hat{\mathbf{y}}) \hat{\mathbf{y}}. \end{aligned} \quad (24b)$$

We denote the position of the dot i by \mathbf{r}_i and that of the connecting site on lead α by \mathbf{r}_α . They are separated by a distance L . The unit vector pointing from dot i to the connecting site on lead α is then denoted by $\hat{\mathbf{g}}^{i\alpha} = (\mathbf{r}_\alpha - \mathbf{r}_i)/L$. In Eq. (24b), $\alpha_{R,D} = k_{R,D}L$ while k_R and k_D are the associated coefficients for the Rashba and (linear) Dresselhaus SOI.

It is well known that an electron acquires a phase when it moves around a loop in a region with SOI.^{2,70,71} In our system the two dots and the two electrodes form a loop. This SOI-induced phase is determined in the following way. Consider the unitary operators $U^L \equiv U^{L1}U^{1R}U^{R2}U^{2L}$, $U^1 \equiv U^{1R}U^{R2}U^{2L}U^{L1}$, $U^R \equiv U^{R2}U^{2L}U^{L1}U^{1R}$ and $U^2 \equiv U^{2L}U^{L1}U^{1R}U^{R2}$, where $U^{\alpha i} = (U^{i\alpha})^\dagger$, which represent the rotations of the spinors related to electrons that traverse around the loop starting and ending at the sites $L, 1, R$ and 2 , respectively. The phase ψ_{so} is obtained by diagonalizing these spin rotations around the loop. The results are formally given by

$$U^x = e^{-i\psi_{\text{so}}} |\hat{\mathbf{n}}_x; +\rangle \langle \hat{\mathbf{n}}_x; +| + e^{i\psi_{\text{so}}} |\hat{\mathbf{n}}_x; -\rangle \langle \hat{\mathbf{n}}_x; -|, \quad (25)$$

for $x = L, R, 1$, and 2 . Here $|\hat{\mathbf{n}}_x; +\rangle$ and $|\hat{\mathbf{n}}_x; -\rangle$ are the spinors for spin up and spin down in the direction $\hat{\mathbf{n}}_x$ defined via $\hat{\mathbf{n}}_x \cdot \boldsymbol{\sigma} |\hat{\mathbf{n}}_x; \pm\rangle = \pm |\hat{\mathbf{n}}_x; \pm\rangle$, where the $\hat{\mathbf{n}}_x$'s are certain real unit vectors in three dimensions. The phase ψ_{so} and the characteristic directions $\hat{\mathbf{n}}_x$'s are fully determined from Eq. (24) and thus incorporate the full information about the SOI-induced spin rotations around the loop. The authors of Ref. [41] have shown that under the spin filter conditions electrons come in with spinor $|\hat{\mathbf{n}}_L; \pm\rangle$ from the left and will go out with spinor $|\hat{\mathbf{n}}_R; \pm\rangle$ on the right (and vice versa). The explicit dependencies of ψ_{so} as well as $\hat{\mathbf{n}}_\alpha$ on the bonding geometry, and on the Rashba and the Dresselhaus coefficients have been discussed in Ref. [41]. Here we replicate in appendix A part of these results that will be used here for the ease of reference.

B. Correspondence to the spinless DQD AB interferometer

1. Decomposition into equivalent spinless systems

Utilizing the eigenspinors of the rotations around the loop, $|\hat{\mathbf{n}}_x; \pm\rangle$, in Eq. (25), the spin rotations along the sections of the loop, Eq. (24), become

$$U^{i\alpha} = \sum_{\nu=\pm} e^{i\psi_{i\alpha}^\nu} |\mathbf{n}_i; \nu\rangle \langle \mathbf{n}_\alpha; \nu|. \quad (26)$$

Here the phases $\psi_{i\alpha}^\pm$'s are restrained by

$$\pm \psi_{\text{so}} = \psi_L^\pm - \psi_R^\pm. \quad (27)$$

where $\psi_\alpha^\pm = \psi_{1\alpha}^\pm - \psi_{2\alpha}^\pm$ for $\alpha = L, R$. With the aid of the basis transformation,

$$a_{i\sigma}^\dagger = \sum_{\nu=\pm} \langle \hat{\mathbf{n}}_i; \nu | \sigma \rangle a_{i\hat{\mathbf{n}}_i; \nu}^\dagger, \quad (28a)$$

$$c_{\alpha k\sigma}^\dagger = \sum_{\nu=\pm} \langle \hat{\mathbf{n}}_\alpha; \nu | \sigma \rangle c_{\alpha k\hat{\mathbf{n}}_\alpha; \nu}^\dagger, \quad (28b)$$

for arbitrary spinor $|\sigma\rangle$, the total Hamiltonian of the system can be decomposed into two terms,

$$\mathcal{H} = \mathcal{H}_+ + \mathcal{H}_-, \quad (29a)$$

where,

$$\mathcal{H}_\pm = \mathcal{H}_S^\pm + \mathcal{H}_E^\pm + \mathcal{H}_T^\pm, \quad (29b)$$

in which

$$\mathcal{H}_S^\pm = \sum_{i=1}^2 E_i a_{i\hat{\mathbf{n}}_i; \pm}^\dagger a_{i\hat{\mathbf{n}}_i; \pm}, \quad (29c)$$

$$\mathcal{H}_E^\pm = \sum_{\alpha k} \epsilon_{\alpha k} c_{\alpha k\hat{\mathbf{n}}_\alpha; \pm}^\dagger c_{\alpha k\hat{\mathbf{n}}_\alpha; \pm}, \quad (29d)$$

and

$$\mathcal{H}_T^\pm = \sum_{i\alpha k} [\bar{V}_{i\alpha k} e^{i\varphi_{i\alpha}^\pm} a_{i\hat{\mathbf{n}}_i; \pm}^\dagger c_{\alpha k\hat{\mathbf{n}}_\alpha; \pm} + \text{h.c.}], \quad (29e)$$

with

$$\varphi_{i\alpha}^\pm = \phi_{i\alpha} + \psi_{i\alpha}^\pm. \quad (29f)$$

Defining similarly $\varphi_\alpha^\pm = \varphi_{1\alpha}^\pm - \varphi_{2\alpha}^\pm$, one directly obtains from Eqs. (23, 27, 29f) that

$$\varphi_\pm \equiv \phi \pm \psi_{\text{so}} = \varphi_L^\pm - \varphi_R^\pm. \quad (30)$$

The \pm subscript in φ_\pm should not be confused with that on the operator $a_{i\hat{\mathbf{n}}_i; \pm}$. The former distinguishes between the two phases in Eq. (30), while the latter denotes the spin polarization along the dot-dependent direction $\hat{\mathbf{n}}_i$.

The phase relation, Eq. (30), in comparison to Eq. (23), reveals that the decomposed Hamiltonian, \mathcal{H}_\pm , Eq. (29), is the Hamiltonian for a spinless DQD AB interferometer with the flux replaced by φ_\pm as the effective flux. Furthermore, by the orthogonality, $\langle \hat{\mathbf{n}}_x; \pm | \hat{\mathbf{n}}_x; \mp \rangle = 0$, these two component Hamiltonians commute with each other,

$$[\mathcal{H}_+, \mathcal{H}_-] = 0. \quad (31)$$

It is therefore possible to relate the spin-resolved currents for the target system to the currents for the effective spinless setup.

2. *Relating the spin-resolved currents to the currents for the spinless DQD AB interferometer*

Consider an arbitrary spinor $|\hat{\mathbf{n}}; \pm\rangle$, defined as the eigenstate of $\hat{\mathbf{n}} \cdot \boldsymbol{\sigma}$, where $\hat{\mathbf{n}}$ is an arbitrary three-dimensional unit vector, by $\hat{\mathbf{n}} \cdot \boldsymbol{\sigma} |\hat{\mathbf{n}}; \pm\rangle = \pm |\hat{\mathbf{n}}; \pm\rangle$. Taking $|\sigma\rangle = |\hat{\mathbf{n}}; \pm\rangle$ in Eq. (6), the spin-resolved current on the lead α with the spinor $|\hat{\mathbf{n}}; \pm\rangle$ is given by

$$I_{\alpha\hat{\mathbf{n}};\pm}(t) = -\frac{d}{dt} \sum_{\mathbf{k} \in \alpha} \text{tr}_{\text{tot}} [c_{\alpha\mathbf{k},\hat{\mathbf{n}};\pm}^\dagger c_{\alpha\mathbf{k},\hat{\mathbf{n}};\pm} \rho_{\text{tot}}(t)]. \quad (32)$$

Setting $\hat{\mathbf{n}} = \hat{\mathbf{n}}_\alpha$ in Eq. (32), with the help of the property, Eq. (31), one is led to

$$I_{\alpha\hat{\mathbf{n}}_\alpha;\pm}(t) = \text{Tr}_{\text{tot}} \left[\hat{I}_{\alpha\hat{\mathbf{n}}_\alpha;\pm}(t) \rho_{\text{tot}}(t_0) \right], \quad (33a)$$

where

$$\hat{I}_{\alpha\hat{\mathbf{n}}_\alpha;\pm}(t) = e^{i\mathcal{H}_\pm(t-t_0)} \hat{I}_{\alpha\hat{\mathbf{n}}_\alpha;\pm} e^{-i\mathcal{H}_\pm(t-t_0)}. \quad (33b)$$

is the Heisenberg representation of the current operator,

$$\hat{I}_{\alpha\hat{\mathbf{n}}_\alpha;\pm} = -i \sum_{\mathbf{k} \in \alpha} [\bar{V}_{i\alpha\mathbf{k}} e^{i\varphi_{i\alpha}^\pm} a_{i\hat{\mathbf{n}}_\alpha;\pm}^\dagger c_{\alpha\mathbf{k}\hat{\mathbf{n}}_\alpha;\pm} - \text{h.c.}]. \quad (33c)$$

On the other hand, the current on lead α for the spinless interferometer described by \mathcal{H}_\pm with the effective flux φ_\pm , is defined by

$$I_\alpha^0(\varphi_\pm, t) = -\frac{d}{dt} \sum_{\mathbf{k} \in \alpha} \text{tr}_{\text{tot}} [c_{\alpha\mathbf{k}\hat{\mathbf{n}}_\alpha;\pm}^\dagger c_{\alpha\mathbf{k}\hat{\mathbf{n}}_\alpha;\pm} \bar{\rho}_{\text{tot}}^\pm(t)], \quad (34)$$

where $\bar{\rho}_{\text{tot}}^\pm(t)$ is the total density matrix for the spinless system \mathcal{H}_\pm . Similarly, Eq. (34) can be rewritten as

$$I_\alpha^0(\varphi_\pm, t) = \text{Tr}_{\text{tot}} \left[\hat{I}_\alpha^\pm(t) \bar{\rho}_{\text{tot}}^\pm(t_0) \right], \quad (35a)$$

where

$$\hat{I}_\alpha^\pm(t) = e^{i\mathcal{H}_\pm(t-t_0)} \hat{I}_\alpha^\pm e^{-i\mathcal{H}_\pm(t-t_0)}. \quad (35b)$$

The current operator in Eq. (35b) is just

$$\hat{I}_\alpha^\pm = \hat{I}_{\alpha\hat{\mathbf{n}}_\alpha;\pm}, \quad (36)$$

which is given by Eq. (33c).

Here we want to study the spin polarization processes induced by the intrinsic mechanisms of SOI, without the inference of the polarization prepared in the initial states. We hence set $\rho_{\text{tot}}(t_0)$ to describe an unpolarized interferometer with the reservoirs in the thermal equilibrium states. Therefore, one can designate $\bar{\rho}_{\text{tot}}^\pm(t_0)$ to be the corresponding initial states for the effective spinless systems such that the following identity,

$$I_{\alpha\hat{\mathbf{n}}_\alpha;\pm}(t) = I_\alpha^0(\varphi_\pm, t), \quad (37)$$

is held for all time t . The identification, Eq. (37), enables us to discuss the spin-dependent transport in the

present system in terms of what has been discussed for the spinless DQD AB interferometer previously.⁶⁹ In the steady-state limit, where the initial preparation for the part of the DQD no longer matters, the identity Eq. (37) with $t \rightarrow \infty$ shall always be held. We will verify Eq. (37) for both the cases of finite times and the steady-state limit in section III D through the explicit use of the formalism presented in Sec. II.

The equality, Eq. (37), means that $I_\alpha^0(\varphi_+, t)$ and $I_\alpha^0(\varphi_-, t)$ respectively are the currents in lead α for spin-up and spin-down electrons in the characteristic direction $\hat{\mathbf{n}}_\alpha$. Using the basis transformation, Eq. (28), with the identification, Eq. (37), the spin-resolved current on lead α for an arbitrary spinor, $|\hat{\mathbf{n}}; \boldsymbol{\nu}\rangle$, defined by Eq. (32), can be expressed as

$$I_{\alpha\hat{\mathbf{n}};\boldsymbol{\nu}}(t) = \sum_{\boldsymbol{\nu}'=\pm} |\langle \hat{\mathbf{n}}_\alpha; \boldsymbol{\nu}' | \hat{\mathbf{n}}; \boldsymbol{\nu} \rangle|^2 I_\alpha^0(\varphi_{\boldsymbol{\nu}'}, t). \quad (38)$$

The current formula, Eq. (38), shows that $I_{\alpha\hat{\mathbf{n}};\boldsymbol{\nu}}(t)$ is a mixture of the currents $I_{\alpha\hat{\mathbf{n}}_\alpha;\pm}(t)$ weighted by the spinor projections $|\langle \hat{\mathbf{n}}_\alpha; \pm | \hat{\mathbf{n}}; \boldsymbol{\nu} \rangle|^2$. The arbitrary global phases embedded in $|\hat{\mathbf{n}}; \boldsymbol{\nu}\rangle$ and $|\hat{\mathbf{n}}_\alpha; \pm\rangle$ are canceled in Eq. (38). From either Eq. (37) or Eq. (38), we find that the spin-independent total current,

$$\begin{aligned} I_\alpha(t) &\equiv I_{\alpha\hat{\mathbf{n}};+}(t) + I_{\alpha\hat{\mathbf{n}};-}(t) \\ &= I_\alpha^0(\varphi_+, t) + I_\alpha^0(\varphi_-, t), \end{aligned} \quad (39)$$

is the sum of these two currents $I_\alpha^0(\varphi_+, t)$ and $I_\alpha^0(\varphi_-, t)$. This is consistent with the analysis in Ref. [71].

C. The rise of spin-polarized transport

The main purpose of the present work is to explore the dynamical rise of the spin polarization in the currents. This is intimately related to the dynamics of spin flows. The spin flow from lead α is

$$\mathbf{I}_\alpha^{\text{S}}(t) = -\frac{d}{dt} \text{tr}_{\text{tot}} [\mathbf{S}_\alpha \rho_{\text{tot}}(t)], \quad (40a)$$

where the total spin operator for the electrode α (with $\hbar = 1$) is defined by,

$$\mathbf{S}_\alpha = \sum_{\mathbf{k} \in \alpha} \sum_{\sigma\sigma'} c_{\alpha\mathbf{k}\sigma}^\dagger \left(\frac{1}{2} \boldsymbol{\sigma} \right)_{\sigma\sigma'} c_{\alpha\mathbf{k}\sigma'}. \quad (40b)$$

Comparing Eq. (40) with Eq. (32), the spin flow from lead α is related to the spin-resolved currents there by

$$\mathbf{I}_\alpha^{\text{S}}(t) = \frac{1}{2} \sum_{i=1}^3 \hat{\mathbf{x}}_i (I_{\alpha\hat{\mathbf{x}}_i;+}(t) - I_{\alpha\hat{\mathbf{x}}_i;-}(t)), \quad (41)$$

where $\{\hat{\mathbf{x}}_1, \hat{\mathbf{x}}_2, \hat{\mathbf{x}}_3\} = \{\hat{\mathbf{x}}, \hat{\mathbf{y}}, \hat{\mathbf{z}}\}$. Using the identities $|\langle \hat{\mathbf{n}}'; \pm | \hat{\mathbf{n}}; \pm \rangle|^2 = (1 + \hat{\mathbf{n}} \cdot \hat{\mathbf{n}}')/2$ and $|\langle \hat{\mathbf{n}}'; \pm | \hat{\mathbf{n}}; \mp \rangle|^2 =$

$(1 - \hat{\mathbf{n}} \cdot \hat{\mathbf{n}}')/2$ for arbitrary directions $\hat{\mathbf{n}}$ and $\hat{\mathbf{n}}'$ in Eq. (38), we can rewrite Eq. (41) as

$$\mathbf{I}_\alpha^S(t) = \frac{\hat{\mathbf{n}}_\alpha}{2} [I_{\alpha\hat{\mathbf{n}}_\alpha;+}(t) - I_{\alpha\hat{\mathbf{n}}_\alpha;-}(t)]. \quad (42)$$

At the same time, Eq. (38) becomes

$$I_{\alpha\hat{\mathbf{n}};\pm}(t) = \frac{I_\alpha(t)}{2} \pm \mathbf{I}_\alpha^S(t) \cdot \hat{\mathbf{n}}. \quad (43)$$

The factors behind the rise of spin-polarized transports can be read from the expression, Eq. (43). Without the SOI, $\psi_{\text{so}} = 0$ and consequently $I_\alpha^0(\varphi_+, t) = I_\alpha^0(\varphi_-, t) = I_\alpha^0(\phi, t)$, Eq. (43) reduces to $I_{\alpha\hat{\mathbf{n}};+}(t) = I_{\alpha\hat{\mathbf{n}};-}(t) = I_\alpha^0(\phi, t)$ for arbitrary $\hat{\mathbf{n}}$. Therefore without SOI it is not possible to have spin flow in this system, as expected. Only when SOI is present, the effective fluxes φ_+ and φ_- can be different. The expression, Eq. (43), together with Eq. (37), manifests that because spin-up electrons and spin-down electrons experience different effective fluxes φ_+ and φ_- , it is possible to have $\mathbf{I}_\alpha^S(t) \neq 0$. This underlies the occurrence of a preferred spin direction in the currents. Note that in the steady-state limit, $t \rightarrow \infty$, the two-terminal spinless interferometers are subjected to phase rigidity, $I_\alpha^0(\varphi) = I_\alpha^0(-\varphi)$. If there is no applied flux, $\phi = 0$, then $\varphi_\pm = \pm\psi_{\text{so}}$ and therefore $I_\alpha^0(\varphi_+) = I_\alpha^0(\varphi_-)$ and $\mathbf{I}_\alpha^S = 0$. This demonstrates the importance of the combined effect of the flux and the SOI for maintaining spin polarization in the currents to the steady-state limit. We will give also explicit calculations showing this result in later sections.

A very important consequence of Eq. (43) is that whenever there is a non-vanishing spin current $\mathbf{I}_\alpha^S(t) \neq 0$, the current on lead α is always polarized in the characteristic direction $\hat{\mathbf{n}}_\alpha$ for all time t , which is fixed by the SOI parameters of the system. Henceforth, to obtain a fully spin-polarized current, one requires either $I_{\alpha\hat{\mathbf{n}}_\alpha;+}(t)$ or $I_{\alpha\hat{\mathbf{n}}_\alpha;-}(t)$ to vanish. The relation of Eq. (37) indicates that such a task could be fulfilled by making one of the currents for the effective spinless systems, $I_\alpha^0(\varphi_+, t)$ and $I_\alpha^0(\varphi_-, t)$, diminish while the other remains finite. Note that since generally $\hat{\mathbf{n}}_L \neq \hat{\mathbf{n}}_R$, the current on the left and that on the right are polarized along different directions.

It is pointed out in Ref. [41] that such a system can give rise to full spin polarization when two conditions are fulfilled. The first condition is that the upper arm and the lower arm of the interferometer are symmetrically set up, namely,

$$\bar{V}_{1\alpha\mathbf{k}} = \bar{V}_{2\alpha\mathbf{k}} = \bar{V}_{\alpha\mathbf{k}}, \quad (44a)$$

$$E_1 = E_2 = E. \quad (44b)$$

The second condition is that the applied magnetic flux and the underlying SOI parameters should be chosen to satisfy

$$\cos(\varphi_-) = -1. \quad (44c)$$

These conditions are obtained from a scattering analysis with a tight-binding modeling of the two leads. Indeed, applying these conditions to the total Hamiltonian

of the target system, we confirm that their validity is independent of the energy dispersion in the leads. We also find that the rise of the fully spin-polarized transport is equivalent to a completely destructive interference in the corresponding spinless interferometer, described by \mathcal{H}_- . Such effects can be seen by analyzing the component Hamiltonians \mathcal{H}_\pm in the decomposition, Eq. (29).

To highlight the role played by the effective flux, we perform a gauge transformation to the Hamiltonians \mathcal{H}_\pm , yielding

$$\mathcal{H}_S^\pm = \sum_{i=1}^2 E_i d_{i\hat{\mathbf{n}}_i;\pm}^\dagger d_{i\hat{\mathbf{n}}_i;\pm}, \quad (45a)$$

$$\mathcal{H}_E^\pm = \sum_{\alpha\mathbf{k}} \epsilon_{\alpha\mathbf{k}} a_{\alpha\mathbf{k}\hat{\mathbf{n}}_\alpha;\pm}^\dagger a_{\alpha\mathbf{k}\hat{\mathbf{n}}_\alpha;\pm}, \quad (45b)$$

and

$$\begin{aligned} \mathcal{H}_T^\pm = & \sum_{\mathbf{k}} [(\bar{V}_{1L\mathbf{k}} e^{i\varphi_\pm/4} d_{1\hat{\mathbf{n}}_1;\pm}^\dagger + \bar{V}_{2L\mathbf{k}} e^{-i\varphi_\pm/4} d_{2\hat{\mathbf{n}}_2;\pm}^\dagger) a_{L\mathbf{k}\hat{\mathbf{n}}_\alpha;\pm} \\ & + (\bar{V}_{1R\mathbf{k}} e^{-i\varphi_\pm/4} d_{1\hat{\mathbf{n}}_1;\pm}^\dagger + \bar{V}_{2R\mathbf{k}} e^{i\varphi_\pm/4} d_{2\hat{\mathbf{n}}_2;\pm}^\dagger) a_{R\mathbf{k}\hat{\mathbf{n}}_R;\pm}] \\ & + \text{h.c.}, \end{aligned} \quad (45c)$$

where the newly defined operators and amplitudes are

$$\begin{aligned} d_{1\hat{\mathbf{n}}_1;\pm}^\dagger &= e^{i\chi_\pm/2} a_{1\hat{\mathbf{n}}_1;\pm}^\dagger, \quad d_{2\hat{\mathbf{n}}_2;\pm}^\dagger = e^{-i\chi_\pm/2} a_{2\hat{\mathbf{n}}_2;\pm}^\dagger, \\ a_{L\mathbf{k}\hat{\mathbf{n}}_L;\pm} &= e^{i\delta\theta_\pm} c_{L\mathbf{k}\hat{\mathbf{n}}_L;\pm}, \quad b_{R\mathbf{k}\hat{\mathbf{n}}_R;\pm} = e^{-i\delta\theta_\pm} c_{R\mathbf{k}\hat{\mathbf{n}}_R;\pm} \end{aligned} \quad (46a)$$

and

$$\bar{V}_{i\alpha\mathbf{k}} = \bar{V}_{i\alpha\mathbf{k}} e^{i\theta_\pm}, \quad (46b)$$

in which the free gauges are

$$\begin{aligned} \chi_\pm &= (\varphi_L^\pm + \varphi_R^\pm)/2, \\ \delta\theta_\pm &= (\theta_L - \theta_R)/4, \\ \bar{\theta}_\pm &= (\theta_L + \theta_R)/4, \end{aligned} \quad (46c)$$

with $\theta_\alpha = \varphi_{1\alpha}^\pm + \varphi_{2\alpha}^\pm$.

Applying the condition, Eq. (44a), the tunneling parts in the Hamiltonians \mathcal{H}_+ and \mathcal{H}_- , can be written as,

$$\mathcal{H}_T^\pm = \mathcal{H}_T^{L\pm} + \mathcal{H}_T^{R\pm}, \quad (47a)$$

where

$$\mathcal{H}_T^{\alpha\pm} = \left[\sum_{\mathbf{k} \in \alpha} \bar{V}_{\alpha\mathbf{k}} \bar{d}_{\alpha\pm}^\dagger a_{\alpha\mathbf{k}\hat{\mathbf{n}}_\alpha;\pm} + \text{h.c.} \right] \sqrt{2}, \quad (47b)$$

with

$$\begin{aligned} \bar{d}_{L\pm}^\dagger &= (e^{i\varphi_\pm/4} d_{1\hat{\mathbf{n}}_1;\pm}^\dagger + e^{-i\varphi_\pm/4} d_{2\hat{\mathbf{n}}_2;\pm}^\dagger) / \sqrt{2}, \\ \bar{d}_{R\pm}^\dagger &= (e^{-i\varphi_\pm/4} d_{1\hat{\mathbf{n}}_1;\pm}^\dagger + e^{i\varphi_\pm/4} d_{2\hat{\mathbf{n}}_2;\pm}^\dagger) / \sqrt{2}, \end{aligned} \quad (47c)$$

where the factor $1/\sqrt{2}$ is for normalization. This shows that for \mathcal{H}_\pm the left and the right electrodes respectively couple to the modes $|L\pm\rangle = \tilde{d}_{L\pm}^\dagger|0\rangle$ and $|R\pm\rangle = \tilde{d}_{R\pm}^\dagger|0\rangle$, where $|0\rangle$ denotes the empty state of the DQD. The overlap between them is

$$\langle L\pm | R\pm\rangle = \sqrt{\frac{\cos(\varphi_\pm) + 1}{2}}. \quad (47d)$$

When φ_- satisfies Eq. (44c), these two modes become orthogonal. By further setting the on-site energies of the DQD to be degenerate, Eq. (44b), the effective spinless system described by \mathcal{H}_- is actually split into two separate systems, each of which is a single-level dot coupled to a reservoir (see Fig. 2(a)). The current on lead α , $I_\alpha^0(\varphi_-, t)$, in this disconnected setup will eventually reach zero. This picture of disconnected electrodes underlies the completely destructive interference for the spinless interferometer. This effect in turn gives the vanishing steady-state current,

$$I_{\alpha\hat{\mathbf{n}}_\alpha;-}(t \rightarrow \infty) = 0, \quad (48)$$

for the spinor $|\hat{\mathbf{n}}_\alpha;- \rangle$ in lead α .

By the same token, the effective configuration for the connection between the two reservoirs for \mathcal{H}_+ is controlled by the value of φ_+ . As long as φ_+ does not satisfy $\cos(\varphi_+) = -1$, the two electrodes for \mathcal{H}_+ stay connected, supporting a non-vanishing current,

$$I_{\alpha\hat{\mathbf{n}}_\alpha;+}(t \rightarrow \infty) \neq 0, \quad (49)$$

provided that a nonzero bias is applied. Noticeably, when $\varphi_+ = 2m\pi$ with m being an arbitrary integer, then the overlap between the two modes, $|L+\rangle$ and $|R+\rangle$ becomes unity. This means that, at degeneracy, the transport only goes through one mode, which is a linear combination of the original two QD's charge states of equal weights.⁷⁴ This opposite limit is contrasted in Fig. 2(b).

The difference between the effective configurations for \mathcal{H}_- and \mathcal{H}_+ has led to the different dependencies of the dynamical evolutions of the currents $I_{\alpha\hat{\mathbf{n}}_\alpha;-}(t)$ and $I_{\alpha\hat{\mathbf{n}}_\alpha;+}(t)$ on the target system's parameters. The configuration of Fig. 2(a) implies that the current carrying the characteristic spinor $|\hat{\mathbf{n}}_\alpha;- \rangle$ in lead α is only affected by the parameters concerning the reservoir α and its coupling to the DQD, whereas the opposite reservoir $\bar{\alpha}$ exerts no influence. On the contrary, for \mathcal{H}_+ , the connected configuration asserts that $I_{\alpha\hat{\mathbf{n}}_\alpha;+}(t)$ is affected by couplings to both of the reservoirs and their respective structures, Fig. 2(b). Explicit calculations of these spin-resolved currents demonstrating such effects will be given in later sections.

D. Real-time spin-dependent currents in terms of the Green functions

In this subsection we apply our previously developed approach, summarized in section II, to the specific system introduced in section III A. The relation between the

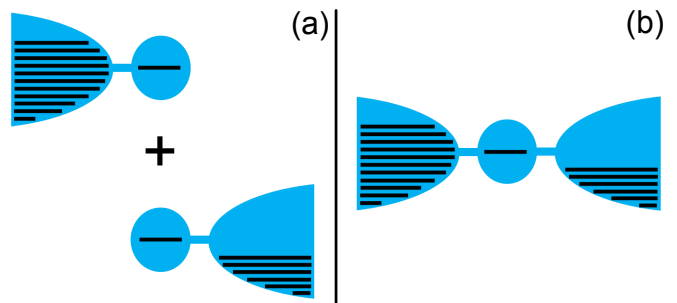


FIG. 2: (color online) Illustration of the effective spinless configuration mapped from the case of having fully polarized transport current. (a) Two separate systems, each of which is a single-level dot coupled to a reservoir. (b) a single-level dot coupled to two reservoirs.

spin-dependent properties in the target system and the properties of the corresponding spinless systems with effective fluxes is clearly revealed from the structure of the Green functions.

1. The Green functions $\mathbf{u}(\tau)$ and $\mathbf{v}(\tau)$

The dynamics of the Green functions on the DQD is influenced by the self-energy induced by the coupling to the leads. The DQD contains four single-electron states, $|i\sigma\rangle$, with $i = 1, 2$ and $\sigma = \pm 1$. Therefore, the level-broadening function, Eq. (12b), as well as the Green functions, $\mathbf{u}(\tau)$ and $\mathbf{v}(\tau)$, are all 4×4 matrices. These 4×4 matrices contain four blocks that are 2×2 matrices in the spin space. A matrix element, for example, is written as, $[\mathbf{u}(\tau)]_{i\sigma,j\sigma'} = \langle \sigma | [\mathbf{u}(\tau)]_{ij} | \sigma' \rangle$. Here $[\mathbf{u}(\tau)]_{ij}$ is a 2×2 matrix in the spin space.

Explicitly, with the property given by Eq. (22), the blocks in the level-broadening function, Eq. (12b), read

$$[\mathbf{\Gamma}^{\alpha\sigma}(\omega)]_{ij} = [\bar{\mathbf{\Gamma}}^\alpha(\omega)]_{ij} e^{i(\phi_{i\alpha} - \phi_{j\alpha})} U^{i\alpha} |\sigma\rangle \langle \sigma| U^{\alpha j}, \quad (50a)$$

where the operator, $U^{i\alpha} |\sigma\rangle \langle \sigma| U^{\alpha j}$, acts on the spin space and the spin-independent level-broadening function is given by

$$[\bar{\mathbf{\Gamma}}^\alpha(\omega)]_{ij} = 2\pi \sum_{k \in \alpha} \bar{V}_{i\alpha k} \bar{V}_{j\alpha k}^* \delta(\omega - \varepsilon_{\alpha k}). \quad (50b)$$

We have already separated out the AB phase from the definition of Eq. (50b). Consequently, the blocks in the self-energies of Eqs. (14a, 14b) are given by

$$\begin{aligned} [\mathbf{g}(\tau)]_{ij} &= \sum_{\alpha=L,R} \sum_{\nu=\pm} [\mathbf{g}_\alpha^\nu(\tau)]_{ij} |\hat{\mathbf{n}}_i; \nu\rangle \langle \hat{\mathbf{n}}_j; \nu|, \\ [\tilde{\mathbf{g}}(\tau)]_{ij} &= \sum_{\alpha=L,R} \sum_{\nu=\pm} [\tilde{\mathbf{g}}_\alpha^\nu(\tau)]_{ij} |\hat{\mathbf{n}}_i; \nu\rangle \langle \hat{\mathbf{n}}_j; \nu|, \end{aligned} \quad (51)$$

where

$$[\mathbf{g}_\alpha^\pm(\tau)]_{ij} = [\bar{\mathbf{g}}_\alpha(\tau)]_{ij} e^{i(\varphi_{i\alpha}^\pm - \varphi_{j\alpha}^\pm)}, \quad (52a)$$

$$[\tilde{\mathbf{g}}_\alpha^\pm(\tau)]_{ij} = [\tilde{\bar{\mathbf{g}}}_\alpha(\tau)]_{ij} e^{i(\varphi_{i\alpha}^\pm - \varphi_{j\alpha}^\pm)}, \quad (52b)$$

with

$$\bar{\mathbf{g}}_\alpha(\tau) = \int \frac{d\omega}{2\pi} \bar{\Gamma}^\alpha(\omega) e^{-i\omega\tau}, \quad (52c)$$

$$\tilde{\bar{\mathbf{g}}}_\alpha(\tau) = \int_{-\infty}^{\infty} \frac{d\omega}{2\pi} f_\alpha(\omega) \bar{\Gamma}^\alpha(\omega) e^{-i\omega\tau}. \quad (52d)$$

Here we assume that the electron reservoirs are initially not polarized at all, so that the initial states for spin up and spin down electrons in each lead α are described by the same Fermi functions $f_\alpha(\omega) = 1/[e^{(\omega - \mu_\alpha)/k_B T} + 1]$ with chemical potential μ_α and temperature T . Note that in Eq. (51), the objects made of spinors, $|\hat{\mathbf{n}}_i; \pm\rangle \langle \hat{\mathbf{n}}_j; \pm|$, act on the spin space. $[\mathbf{g}_\alpha^\pm(\tau)]_{ij}$ and $[\tilde{\mathbf{g}}_\alpha^\pm(\tau)]_{ij}$ are the elements of the 2×2 matrices, $\mathbf{g}_\alpha^\pm(\tau)$ and $\tilde{\mathbf{g}}_\alpha^\pm(\tau)$ respectively, where i, j run over the charge states in the DQD.

Correspondingly, the blocks in the retarded Green function, $\mathbf{u}(\tau)$ [see Eq. (13a)] and correlation Green function, $\mathbf{v}(\tau)$, [see Eq. (13b) and Eq. (15)], are given

by,

$$\begin{aligned} [\mathbf{u}(\tau)]_{ij} &= \sum_{\nu=\pm} [\mathbf{u}^\nu(t, \tau)]_{ij} |\hat{\mathbf{n}}_i; \nu\rangle \langle \hat{\mathbf{n}}_j; \nu|, \\ [\mathbf{v}(\tau)]_{ij} &= \sum_{\nu=\pm} [\mathbf{v}^\nu(\tau)]_{ij} |\hat{\mathbf{n}}_i; \nu\rangle \langle \hat{\mathbf{n}}_j; \nu|. \end{aligned} \quad (53a)$$

where the 2×2 matrices $\mathbf{u}^\pm(\tau)$ and $\mathbf{v}^\pm(\tau)$ satisfy the equations,

$$\partial_\tau \mathbf{u}^\pm(\tau) + i\mathbf{E}\mathbf{u}^\pm(\tau) + \int_{t_0}^\tau d\tau' \mathbf{g}^\pm(\tau - \tau') \mathbf{u}^\pm(\tau') = 0, \quad (53b)$$

and

$$\mathbf{v}^\pm(\tau) = \int_{t_0}^\tau d\tau_1 \int_{t_0}^{\tau_1} d\tau_2 \mathbf{u}^\pm(\tau - \tau_1) \tilde{\mathbf{g}}^\pm(\tau_1 - \tau_2) \bar{\mathbf{u}}^\pm(\tau_2), \quad (53c)$$

with $\mathbf{g}^\pm(\tau) = \sum_\alpha \mathbf{g}_\alpha^\pm(\tau)$, $\tilde{\mathbf{g}}^\pm(\tau) = \sum_\alpha \tilde{\mathbf{g}}_\alpha^\pm(\tau)$ and $\bar{\mathbf{u}}^\pm(\tau) = \mathbf{u}^\pm(t - \tau + t_0)^\dagger$. The boundary condition $\mathbf{u}^\pm(0) = \mathbf{1}$ is imposed. Here $\mathbf{E} = \begin{pmatrix} E_1 & 0 \\ 0 & E_2 \end{pmatrix}$ is the on-site energy matrix for the DQD. Explicitly, the matrices of the effective self-energies are,

$$\mathbf{g}^\pm(\tau) = \begin{pmatrix} [\bar{\mathbf{g}}_L(\tau)]_{11} + [\bar{\mathbf{g}}_R(\tau)]_{11} & e^{i\chi_\pm} ([\bar{\mathbf{g}}_L(\tau)]_{12} e^{i\varphi_\pm/2} + [\bar{\mathbf{g}}_R(\tau)]_{12} e^{-i\varphi_\pm/2}) \\ e^{-i\chi_\pm} ([\bar{\mathbf{g}}_L(\tau)]_{21} e^{-i\varphi_\pm/2} + [\bar{\mathbf{g}}_R(\tau)]_{21} e^{i\varphi_\pm/2}) & [\bar{\mathbf{g}}_L(\tau)]_{22} + [\bar{\mathbf{g}}_R(\tau)]_{22} \end{pmatrix}, \quad (54)$$

where χ_\pm is an arbitrary gauge phase given in Eq. (46c). Comparing Eq. (54) with that for the spinless DQD AB interferometer in our previous work,⁶⁹ we find the effective Green functions $\mathbf{u}^\pm(\tau)$ and $\mathbf{v}^\pm(\tau)$ here are just those for the corresponding spinless system, but with the flux ϕ replaced by the effective fluxes φ_\pm . The explicit analysis presented above is thus consistent with the correspondence between the target system and the spinless DQD AB interferometer discussed in section III B.

2. The spin-resolved currents

If initially the DQD has no electrons, then by the use of Eq. (20) for the current, we directly obtain the form of Eq. (38), in which

$$\begin{aligned} I_\alpha^0(\varphi_\pm, t) &= 2\text{ReTr} \int_0^t d\tau (\tilde{\mathbf{g}}_\alpha^\pm(t - \tau) \bar{\mathbf{u}}^\pm(\tau) - \mathbf{g}_\alpha^\pm(t - \tau) \mathbf{v}^\pm(\tau)). \end{aligned} \quad (55)$$

The current, Eq. (55), as a physical observable, is shown to be independent of the arbitrary gauge phase χ_\pm that

appear in Eq. (54) (see details in Appendix B). By the one-to-one correspondence on the level of the Green functions $\mathbf{u}^\pm(\tau)$ and $\mathbf{v}^\pm(\tau)$, discussed in a previous subsection, Eq. (55) is exactly the current on lead α for the spinless system described by \mathcal{H}_\pm in Eq. (29) with the effective flux φ_\pm . By taking $\hat{\mathbf{n}} = \hat{\mathbf{n}}_\alpha$ in Eq. (38), together with Eq. (55), one immediately verifies Eq. (37).

The initial preparation of the DQD, deviating from being empty, namely, $\rho^{(1)}(t_0) \neq 0$, only has a temporary effect on the currents, seen from the last term of Eq. (18), before $\mathbf{u}(t)$ goes to zero for large t . In the limit where $\mathbf{u}(t \rightarrow \infty) = 0$, the steady-state value of Eq. (18) is just that of Eq. (20). The latter directly guarantees the validity of Eq. (38) with Eq. (55) which ensures the identification of Eq. (37) in the steady-state limit. For simplicity and for the physical purpose already stated before, we hereafter restrict our discussion to the case $\rho^{(1)}(t_0) = 0$ in what follows.

The Green functions, Eq. (53), together with the current expression, Eq. (55), and the identity, Eq. (37), form the basis of exploring the spin-dependent electron transport described by Eq. (43).

3. Results in the wide-band limit

For explicit calculations, we take the commonly assumed wide-band limit. The effective self-energy functions, Eq.(54), become

$$\mathbf{g}^\pm(\tau) = \delta(\tau) \begin{pmatrix} \Gamma & e^{i\chi_\pm} m_\pm \\ e^{-i\chi_\pm} m_\pm^* & \Gamma \end{pmatrix}, \quad (56)$$

where $m_\pm = (\Gamma_L e^{i\varphi_\pm/2} + \Gamma_R e^{-i\varphi_\pm/2})$. The broadening due to the coupling to electrode α is Γ_α and $\Gamma = \Gamma_L + \Gamma_R$. The retarded Green function \mathbf{u} is now written as

$$\mathbf{u}^\pm(\tau) = u_0(\varphi_\pm, \tau) \sigma_0 - u_p(\varphi_\pm, \tau) \hat{p}(\chi_\pm, \varphi_\pm) \cdot \vec{\sigma} \quad (57a)$$

where σ_0 is a 2×2 identity matrix and

$$\vec{\sigma} = (\sigma_+, \sigma_-, \sigma_z), \quad (57b)$$

is a vector of three Pauli matrices with

$$\sigma_\pm = \sigma_x \pm i\sigma_y. \quad (57c)$$

The space polarization vector is given by

$$\hat{p}(\chi_\pm, \varphi_\pm) = \vec{p}(\chi_\pm, \varphi_\pm) / \Gamma_{\varphi_\pm}, \quad (57d)$$

where

$$\vec{p}(\chi_\pm, \varphi_\pm) = (e^{i\chi_\pm} m_\pm / 2, e^{-i\chi_\pm} m_\pm^* / 2, i\delta E) \quad (57e)$$

and

$$\Gamma_{\varphi_\pm} = \sqrt{\Gamma_L^2 + \Gamma_R^2 + 2\Gamma_L\Gamma_R \cos(\varphi_\pm) - \delta E^2}, \quad (57f)$$

in which $\delta E = E_1 - E_2$. By setting $E_1 + E_2 = 0$ as an energy reference, we are led to

$$u_0(\varphi_\pm, \tau) = \frac{1}{2} \left(e^{-\gamma_{\varphi_\pm}^- \tau} + e^{-\gamma_{\varphi_\pm}^+ \tau} \right), \quad (58a)$$

$$u_p(\varphi_\pm, \tau) = \frac{1}{2} \left(e^{-\gamma_{\varphi_\pm}^- \tau} - e^{-\gamma_{\varphi_\pm}^+ \tau} \right), \quad (58b)$$

where

$$\gamma_{\varphi_\pm}^\pm = \frac{1}{2} \left(\Gamma \pm \Gamma_{\varphi_\pm} \right). \quad (58c)$$

The time needed to reach the steady state is thus determined by the decay rates $\gamma_{\varphi_\pm}^\pm$ which depend on the geometry of the system and on the effective fluxes φ_\pm .

Comparing the above formulae with the spinless DQD AB interferometer in our previous work,⁶⁹ we find a one-to-one correspondence with the replacement of ϕ in Ref. [69] by φ_\pm . Removing SOI we immediately recover the corresponding results in a spinless DQD AB interferometer.

IV. SPIN-DEPENDENT CURRENT IN THE STEADY STATE

Before we proceed to investigate the dynamical processes, we first take the steady-state limit. We examine the conditions for generating spin-polarized current. We reproduce known results about spin polarization. We also discuss other possibilities of spin dependence of the steady-state currents. In the end of this section, we investigate how to extract the spin-polarized transmission from the spin-independent total transmission at various electric and magnetic fields.

A. Spin-polarized currents in the steady state

The spin-resolved current, $I_{\alpha\hat{\mathbf{n}};\pm}(t)$, along an arbitrary direction, $\hat{\mathbf{n}}$, involves both the currents $I_\alpha^0(\varphi_+, t)$ and $I_\alpha^0(\varphi_-, t)$. As seen from Eqs. (58), each of these currents may require a different time to approach its steady state. When $\gamma_{\varphi_\pm}^-$ is nonzero, the time for $I_\alpha^0(\varphi_\pm, t)$ to reach its steady state must be larger than $1/\text{Re}[\gamma_{\varphi_\pm}^-]$. When $\delta E = 0$ and the effective flux φ_\pm is an even multiple of π , then $\gamma_{\varphi_\pm}^- = 0$ and $\gamma_{\varphi_\pm}^+ = \Gamma$. In this case, as discussed previously,⁶⁹ only a single decay channel is present and the corresponding decay rate is just Γ . The time to reach the steady state in this situation must be larger than $1/\Gamma$.

Taking the steady-state limit of Eq. (43), $I_{\alpha\hat{\mathbf{n}};\pm}(t \rightarrow \infty) = I_{\alpha\hat{\mathbf{n}};\pm}^\infty$, the current from the lead α carrying spinor $|\hat{\mathbf{n}}; \pm\rangle$ becomes

$$I_{\alpha\hat{\mathbf{n}};\pm}^\infty = \frac{1}{2} \left[(1 \pm \hat{\mathbf{n}}_\alpha \cdot \hat{\mathbf{n}}) I_\alpha^0(\varphi_+) + (1 \mp \hat{\mathbf{n}}_\alpha \cdot \hat{\mathbf{n}}) I_\alpha^0(\varphi_-) \right] \quad (59a)$$

where

$$I_\alpha^0(\varphi_\pm) = \int \frac{d\omega}{2\pi} (f_\alpha(\omega) - f_{\bar{\alpha}}(\omega)) T^0(\varphi_\pm, \omega), \quad (59b)$$

in which $\bar{\alpha} = R$ if $\alpha = L$ and vice versa. Here the linear response of the effective spinless system with effective flux φ_\pm is given by the transmission,

$$T^0(\varphi_\pm, \omega) = 4\Gamma_L\Gamma_R \frac{\omega^2 \cos^2(\varphi_\pm/2) + (\frac{\delta E}{2} \sin(\varphi_\pm/2))^2}{\left(\omega^2 + (\gamma_{\varphi_\pm}^+)^2\right) \left(\omega^2 + (\gamma_{\varphi_\pm}^-)^2\right)}. \quad (59c)$$

Due to charge conservation, the steady-state currents for the spinless DQD AB interferometer are subjected to

$$I_L^0(\varphi_\pm) = -I_R^0(\varphi_\pm). \quad (60)$$

Using Eq. (37), we immediately find that

$$I_{L\hat{\mathbf{n}}_L;\pm}^\infty = -I_{R\hat{\mathbf{n}}_R;\pm}^\infty. \quad (61)$$

This indicates that the current for spinor $|\hat{\mathbf{n}}_L; \pm\rangle$ leaving the left side is converted to the current for $|\hat{\mathbf{n}}_R; \pm\rangle$ in

the right side. It also reveals the effects of SOI when electrons are transferred across the DQD from one lead to the other. Directly from Eq. (61) or more generally from Eq. (59), we have the total current conversation,

$$I_L = -I_R. \quad (62)$$

Applying the conditions for realizing the full spin-polarization in Eq. (44) to Eq. (59) results in

$$I_{\alpha\hat{\mathbf{n}}\alpha;-}^{\infty} = 0, \quad (63a)$$

$$I_{\alpha\hat{\mathbf{n}}\alpha;+}^{\infty} \neq 0. \quad (63b)$$

Therefore the current on lead α is polarized to carry only the spinor $|\hat{\mathbf{n}}_{\alpha}; +\rangle$ while that for the opposite spinor $|\hat{\mathbf{n}}_{\alpha}; -\rangle$ vanishes. Equations (63), obtained in the wide-band limit, are the same as Eqs. (48,49), deduced independently of the form of the level-broadening function given in section III C. Our results here thus reproduce the findings in Ref. [41].

Given that the two conditions for full polarization are satisfied, the polarized current on lead α is described by

$$I_{\alpha\hat{\mathbf{n}}\alpha;+}^{\infty} = 4\Gamma_L\Gamma_R \int \frac{d\omega}{2\pi} (f_{\alpha}(\omega) - f_{\bar{\alpha}}(\omega)) \times \frac{\omega^2 \cos^2(\varphi_+/2)}{\left(\omega^2 + (\gamma_{\varphi_+}^+)^2\right) \left(\omega^2 + (\gamma_{\varphi_+}^-)^2\right)}. \quad (64)$$

Setting $\mu_L = -\mu_R = eV/2$ at zero temperature, the integral in the above equation can be done explicitly, yielding

$$I_{\alpha\hat{\mathbf{n}}\alpha;+}^{\infty} = \pm \frac{4\Gamma_L\Gamma_R}{\pi\Gamma\Gamma_{\varphi}} \cos^2(\varphi_+/2) \times \left[\gamma_{\varphi_+}^+ \tan^{-1} \left(\frac{eV}{2\gamma_{\varphi_+}^+} \right) - \gamma_{\varphi_+}^- \tan^{-1} \left(\frac{eV}{2\gamma_{\varphi_+}^-} \right) \right], \quad (65)$$

where the overall sign \pm on the right-hand side takes $+$ for $\alpha = L$ and $-$ for $\alpha = R$.

This shows that the magnitude of the fully polarized currents sensitively depend on the effective flux φ_+ mainly through the term $\cos^2(\varphi_+/2)$. When $\psi_{\text{so}} = (2(m-n) + 1)\pi/2$ and $\phi = (2(m+n) - 1)\pi/2$ for arbitrary integers m and n , the fully polarized currents can be maximized with the effective flux $\varphi_+ = 2m\pi$. On the contrary, if $\psi_{\text{so}} = (m-n)\pi$ and $\phi = (m+n-1)\pi$, then $\cos(\varphi_{\pm}) = -1$ and both $I_{\alpha\hat{\mathbf{n}}\alpha;+}$ and $I_{\alpha\hat{\mathbf{n}}\alpha;-}$ vanish. To see what SOI parameters can realize the situations discussed above, we take examples having only Rashba SOI for simplicity. The bonding geometry of the system is specified by the diamond angle, β (see Fig. 1). The dependence of SOI-induced phase ψ_{so} on the Rashba SOI strength α_R and on the diamond angle β is found in Eq. (A1). By Eq. (A1), the maximized full polarization current with $\varphi_+ = 2m\pi$ corresponds to the constraint $\sin^2(\alpha_R) \sin(2\beta) = \sqrt{1/2}$ on α_R and β . The opposite limit where all currents vanish corresponds to the condition $\sin^2(\alpha_R) \sin(2\beta) = 1$.

Opposite to the fully spin-polarized current is the randomly polarized current, namely, $I_{\alpha\hat{\mathbf{n}};+} = I_{\alpha\hat{\mathbf{n}};-}$, for any direction $\hat{\mathbf{n}}$. There are two possibilities for such unpolarized transport to occur. The first is the trivial situation where the SOI is switched off. The currents remain unpolarized not only in the steady-state limit but also throughout the time, as shown in the previous discussion below Eq. (43). The second circumstance is that there is no applied magnetic flux, $\phi = 0$. In this case, we have $\varphi_{\pm} = \pm\psi_{\text{so}}$ and $I_{\alpha}^0(\psi_{\text{so}}) = I_{\alpha}^0(-\psi_{\text{so}})$ due to phase rigidity because the effective spinless interferometer is a two-terminal system [see also Eqs. (59b,59c)]. Putting this into Eq. (59a), one immediately obtains $I_{\alpha\hat{\mathbf{n}};+} = I_{\alpha\hat{\mathbf{n}};-}$, for all directions $\hat{\mathbf{n}}$. This result exemplifies the discussion about the steady-state limit below Eq. (43) in section III C. The currents in the steady-state limit are unpolarized but they may be transiently polarized (see the later discussion in section V B). When one is away from either of the two conditions for full spin polarization, one cannot reach $T^0(\varphi_{\pm}, \omega) = 0$ for all ω . Therefore in general both $I_{\alpha\hat{\mathbf{n}}\alpha;-}$ and $I_{\alpha\hat{\mathbf{n}}\alpha;+}$ are nonzero and the currents are only partially polarized.

B. Extracting spin-resolved transmission from measurement of total transmission

In the absence of the magnetic flux, the line shape of the spin-independent total transmission depends solely on the SOI-induced phase. Therefore one can extract ψ_{so} from the total transmission. This in turn can be used to map out the relations between the values of the transmission for the underlying spinless system and the effective fluxes, $T^0(\varphi, \omega)$.

The spin-independent total charge transport current is defined by

$$I = \frac{1}{2}(I_L - I_R). \quad (66)$$

Using Eq. (59) with Eq. (39), the charge transport current, Eq. (66), in the steady-state limit becomes

$$I = \int \frac{d\omega}{2\pi} (f_L(\omega) - f_R(\omega)) T(\phi, \psi_{\text{so}}, \omega), \quad (67a)$$

where the total charge transmission, $T(\phi, \psi_{\text{so}}, \omega)$, is

$$T(\phi, \psi_{\text{so}}, \omega) = T^0(\varphi_+, \omega) + T^0(\varphi_-, \omega). \quad (67b)$$

The zero bias charge conductance at low temperature, as the linear response, is simply given by $T(\phi, \psi_{\text{so}}, \omega)$ in Eq. (67). By turning off the magnetic flux, the total charge transmission becomes

$$T(\phi = 0, \psi_{\text{so}}, \omega) = 2T^0(\psi_{\text{so}}, \omega), \quad (68)$$

where we have utilized $T^0(\psi_{\text{so}}, \omega) = T^0(-\psi_{\text{so}}, \omega)$.

We discuss separately the cases with $\delta E = 0$ and with $\delta E \neq 0$. By tuning the on-site energies such that $\delta E = 0$,

with $\psi_{\text{so}} = 2n\pi$, where n is an arbitrary integer, Eq. (59c) becomes a Lorentzian line shape,

$$T^0(2n\pi, \omega) = \frac{4\Gamma_L\Gamma_R}{(\omega^2 + \Gamma^2)}, \quad (69)$$

as shown by the most front plot in the left panel of Fig. 3. For $\psi_{\text{so}} \neq 2n\pi$, the single-peak profile splits into two peaks, as shown by the other plots in the left panel of Fig. 3. The separation of the two peaks is given by

$$\Delta\omega = \sqrt{2\Gamma_L\Gamma_R(1 - \cos(\psi_{\text{so}}))}. \quad (70)$$

For $\psi_{\text{so}} = (2n - 1)\pi$, the transmissions vanish, as shown by the most rear plot on the left panel of Fig. 3.

With $\delta E \neq 0$, $T^0(\psi_{\text{so}}, \omega)$ for $\psi_{\text{so}} = 2n\pi$ shows split peaks and its value at $\omega = 0$ equals to zero. This is the most front plot on the right panel of Fig. 3. The separation between the two peaks in this case becomes

$$\Delta\omega = \sqrt{2}|\delta E|. \quad (71)$$

For $\psi_{\text{so}} \neq 2n\pi$, the line shape of the transmission may exhibit two peaks or a single peak profile, depending on the relations between ψ_{so} and the nonzero value of δE . From Eq. (59c), we find that if

$$\begin{aligned} \bar{\gamma}(\psi_{\text{so}}) &\equiv 4\left(\gamma_{\psi_{\text{so}}}^+ \gamma_{\psi_{\text{so}}}^-\right)^2 \cos^2(\psi_{\text{so}}/2) \\ &- \left[\left(\gamma_{\psi_{\text{so}}}^+\right)^2 + \left(\gamma_{\psi_{\text{so}}}^-\right)^2 \right] \delta E^2 \sin^2(\psi_{\text{so}}/2) > 0, \end{aligned} \quad (72)$$

is satisfied, then there emerges a profile with two peaks, as exemplified by the second most front plot on the right panel of Fig. 3. The separation between these two peaks is given by

$$\Delta\omega = \left\{ \frac{-\frac{\delta E^2}{2} \sin^2(\psi_{\text{so}}/2)}{2 \cos^2(\psi_{\text{so}}/2)} + \frac{\sqrt{\left[\frac{\delta E^2}{2} \sin^2(\psi_{\text{so}}/2)\right]^2 + \bar{\gamma}(\psi_{\text{so}}) \cos^2(\psi_{\text{so}}/2)}}{2 \cos^2(\psi_{\text{so}}/2)} \right\}^{1/2}. \quad (73)$$

When the condition, Eq. (72), is not fulfilled, the transmission line shape has a single peak, but it is not a Lorentzian profile (see the plots on the right panel behind the second most front one in Fig. 3). The single peak occurs at $\omega = 0$ with the height

$$T^0(\psi_{\text{so}} \neq 2n\pi, \omega = 0) = \frac{16\Gamma_L\Gamma_R\delta E^2 \sin^2(\psi_{\text{so}}/2)}{[\delta E^2 + 4\Gamma_L\Gamma_R \sin^2(\psi_{\text{so}}/2)]^2}. \quad (74)$$

The height of the peak depends on δE and on ψ_{so} . In particular, when $\delta E = 0$ then Eq. (69) yields the height $4\Gamma_L\Gamma_R/\Gamma^2$.

Therefore by observing the zero bias conductance profile at given electric field without applying the magnetic flux, one can extract the SOI-induced phase ψ_{so} from Eqs. (70-74) at that electric field. The other way around, one can also fix the electric field at which $\psi_{\text{so}} = 2n\pi$, and find out the value of ϕ at a given magnetic field through a similar procedure by the property, $T(\phi, \psi_{\text{so}} = 2n\pi, \omega) = 2T^0(\phi, \omega)$. Using these results, one can map out the dependence of $T^0(\varphi, \omega)$ on the effective flux φ . Together with the knowledge on how ϕ and ψ_{so} depend on the directly tunable magnetic and electric fields, the transmission for polarized current, namely, $T^0(\varphi_+, \omega) - T^0(\varphi_-, \omega)$, at given electric and magnetic fields can be found. In particular, when the full polarization conditions are met, the total transmission shall satisfy $T(\phi, \psi_{\text{so}}, \omega)|_{\varphi_{\mp} = (2n-1)\pi} = T^0(\varphi_{\pm}, \omega)$.

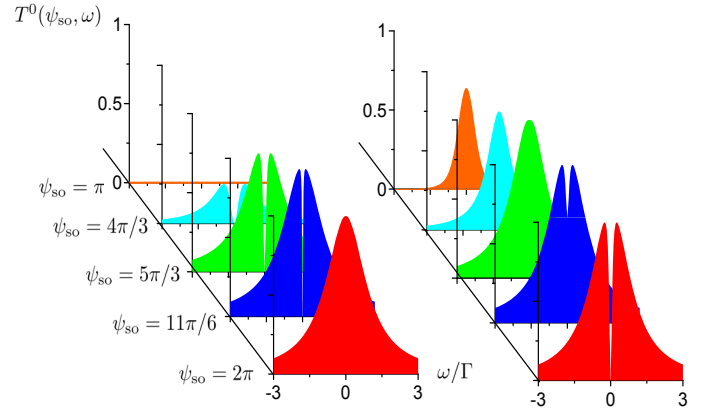


FIG. 3: (color online) The transmission for the effective spinless DQD AB interferometer with the flux set at $\varphi = \psi_{\text{so}}$. The left panel is for $\delta E = 0$ and the right panel is for $\delta E = 0.5\Gamma$. The couplings are $\Gamma_L = \Gamma_R = \Gamma/2$ for both panels. These series of stacked plots show $T^0(\psi_{\text{so}}, \omega)$ versus ω at some specific values of ψ_{so} , as labeled in the figure.

V. DYNAMICS OF SPIN-DEPENDENT TRANSPORT

In this section, we discuss the time evolutions of the spin-dependent transport. In the first subsection we study the real time evolution towards a full spin-polarization in the currents, when the two conditions given above are fulfilled. In the second subsection, we turn to the more general situation to investigate the interplay between the AB and AC interference effects on the dynamics of spin currents. In the third subsection, we discuss how one can obtain the spin-resolved currents from the total charge currents, using approaches similar to those mentioned in a previous section.

A. Time evolution of full spin polarization in currents

We have discussed the requirements for generating polarized currents in the steady-state. However, even when those requirements are satisfied, the currents during the transient processes for both of the orthogonal spinors are generally nonvanishing. Using Eq. (37), we explicitly study how the currents for opposite spins along the characteristic directions in each of the electrodes, $I_{\alpha\hat{\mathbf{n}}_{\alpha};-}(t)$ and $I_{\alpha\hat{\mathbf{n}}_{\alpha};+}(t)$, change in time.

The real-time polarization process is mainly manifested through the evolution of the current $I_{\alpha\hat{\mathbf{n}}_{\alpha};-}(t)$, that will eventually decay to zero. The requirement Eq. (44) has turned Eq. (57f) into $\Gamma_{\varphi_-} = |\Gamma_L - \Gamma_R|$. Substituting this into Eq. (57) and Eq. (53c) with Eq. (56), and using also Eq. (55) with Eq. (37), we get

$$I_{\alpha\hat{\mathbf{n}}_{\alpha};-}(t) = 4\Gamma_{\alpha} \times \int \frac{d\omega}{2\pi} f_{\alpha}(\omega) \frac{e^{-\Gamma_{\alpha}t} (\Gamma_{\alpha} \cos \omega t + \omega \sin \omega t) - \Gamma_{\alpha} e^{-2\Gamma_{\alpha}t}}{\omega^2 + \Gamma_{\alpha}^2}. \quad (75)$$

According to the analysis in section III C, under the condition Eq. (44), the corresponding spinless interferometer, whose current is related to the current carrying the spinor $|\hat{\mathbf{n}}_{\alpha};-\rangle$, has a disconnected effective configuration as that depicted in Fig. 2(a). Comparing Eq. (75) with the current for a spinless single level coupled to a single reservoir, we find they are identical (see Eq. (C1) in appendix C). The result that Eq. (75), as the current for spinor $|\hat{\mathbf{n}}_{\alpha};-\rangle$ on lead α , is not affected by anything from the other lead $\bar{\alpha}$, verifies the conclusion in section III C.

In contrast to the decay of the currents $I_{\alpha\hat{\mathbf{n}}_{\alpha};-}(t)$ toward zero, the time evolution of the currents $I_{\alpha\hat{\mathbf{n}}_{\alpha};+}(t)$ generally depends on parameters from both of the leads. At the optimal point $\varphi_+ = 2m\pi$ leading to $\Gamma_{\varphi_+} = \Gamma$, a similar substitution as used for obtaining Eq. (75) results in,

$$I_{\alpha\hat{\mathbf{n}}_{\alpha};+}(t) = 4\Gamma_{\alpha} \int \frac{d\omega}{2\pi} \left\{ f_{\alpha}(\omega) \frac{\Gamma + (\omega \sin(\omega t) - \Gamma \cos(\omega t)) e^{-\Gamma t}}{\omega^2 + \Gamma^2} - \sum_{\alpha'=L,R} \Gamma_{\alpha'} f_{\alpha'}(\omega) \frac{(1 + e^{-2\Gamma t} - 2 \cos(\omega t) e^{-\Gamma t})}{\omega^2 + \Gamma^2} \right\}. \quad (76)$$

For this part, the corresponding effective spinless configuration discussed in section III C is a single-level dot coupled to two reservoirs, as shown in Fig. 2(b). This is verified by independently calculating the currents for such an effective configuration (comparing Eq. (76) with Eq. (C2)). From Eq. (76), one can also see that $I_{\alpha\hat{\mathbf{n}}_{\alpha};+}(t = t_{ss}) \neq 0$ with nonzero bias, as expected from previous discussions.

Equation (75) indicates that the time for $I_{\alpha\hat{\mathbf{n}}_{\alpha};-}(t)$ to reach its steady-state value is mainly determined by the

term $e^{-\Gamma_{\alpha}t}$. The smaller Γ_{α} is, the slower the full spin-polarization of the current in lead α is reached. On the other hand, one finds from Eq. (76) that the time for $I_{\alpha\hat{\mathbf{n}}_{\alpha};+}(t)$ to reach its steady value is dominated by the term $e^{-\Gamma t}$. Therefore it is insensitive to the specific values taken by the individual couplings Γ_L and Γ_R for a fixed $\Gamma = \Gamma_L + \Gamma_R$. However, the coupling geometry still affects the magnitude of the full spin-polarized current. In the steady states, Eqs. (64,65) show that the spin-polarized current can be enhanced by having larger value of $\Gamma_L \Gamma_R$. Note that Eq. (64) is invariant under the exchange of the couplings, $\Gamma_L \leftrightarrow \Gamma_R$.

In Fig. 4(a1,a2) and (b1,b2), we demonstrate the effects of the coupling geometry discussed above, specified by different values of (Γ_L, Γ_R) , on the time evolution of the spin-resolved currents. The curves in these four plots with the same line styles are with the same pair of couplings (Γ_L, Γ_R) , subject to $\Gamma_L + \Gamma_R = \Gamma$. In Fig. 4 (a1) and (a2), we illustrate the time evolution of $I_{\alpha\hat{\mathbf{n}}_{\alpha};-}(t)$. It shows that a smaller Γ_{α} leads to a slower decay of the current $I_{\alpha\hat{\mathbf{n}}_{\alpha};-}(t)$, thus a slower process of spin-polarization (see the insets for a clearer view). Since we have set $\mu_L > \mu_R$, more electrons are involved in the left than in the right lead. At later times, this results in generally bigger magnitudes of currents in the left (comparing the magnitudes in the insets of Fig. 4(a1) and (a2).)

In Fig. 4 (b1,b2), the time evolutions of $I_{\alpha\hat{\mathbf{n}}_{\alpha};+}(t)$ with $\varphi_+ = 2m\pi$ are inspected. It shows that different coupling geometries result in similar times for $I_{\alpha\hat{\mathbf{n}}_{\alpha};+}(t)$ to reach the corresponding steady-state values. The merging of the curves (blue medium-dashed line merged with green dash-dotted line and black long-dashed line merged with magenta short-dashed line) occur after a time of about $2.5\Gamma^{-1}$, reaching steady-state values proportional to $\Gamma_L \Gamma_R$. The maximized spin-polarized current is found with $\Gamma_L = \Gamma_R = \Gamma/2$. Comparing Fig. 4 (b) with Fig. 4 (a) insets, one finds that $I_{\alpha\hat{\mathbf{n}}_{\alpha};+}(t)$ reaches a stable value generally faster than the full spin-polarization is arrived. This is because the rate for the former, $\Gamma = \Gamma_L + \Gamma_R$, as a sum of two couplings, is larger than the rate for the latter, Γ_L or Γ_R . The different dependencies of the dynamical processes of the currents $I_{\alpha\hat{\mathbf{n}}_{\alpha};-}(t)$ and $I_{\alpha\hat{\mathbf{n}}_{\alpha};+}(t)$ on the couplings to the reservoirs, discussed in section III C, is then illustrated here.

We further investigate the behavior of $I_{\alpha\hat{\mathbf{n}}_{\alpha};+}(t)$ when the system is set away from the optimal point $\varphi_+ = 2m\pi$. In Fig. 4(c1,c2), the time evolution of $I_{\alpha\hat{\mathbf{n}}_{\alpha};+}(t)$ with different effective fluxes φ_+ are plotted. When φ_+ is placed away from $2m\pi$ toward $(2m+1)\pi$, the steady-state value of this current, proportional to $\cos^2(\varphi_+/2)$, as inspected from Eq. (64), decreases. Figure 4(c1,c2) also shows that the value of φ_+ does not obviously affect the time to approach the steady state but it influences the overall magnitudes of $I_{\alpha\hat{\mathbf{n}}_{\alpha};+}(t)$ throughout the time evolution. Note that different values of φ_+ are realized by applying different magnetic fluxes and SOI parameters. As long as the choices of the magnetic fluxes and SOI parameters are subjected to Eq. (44c), the time dependence of

$I_{\alpha\hat{n}_\alpha;-}(t)$ remains the same as described by Eq. (75).

The spin polarization processes of the currents are alternatively presented in Fig. 5, which displays the spin-independent total charge currents, $I_\alpha(t)$ (see Eq. (39)), and the spin currents, $\mathbf{I}_\alpha^S(t)$ [see Eq. (42)]. Since the spin-down current $I_{\alpha\hat{n}_\alpha;-}(t)$ will vanish in the steady state, both $I_\alpha(t)$ and $\mathbf{I}_\alpha^S(t)$ will eventually approach $I_{\alpha\hat{n}_\alpha;+}(t)$ at long times. The effects of coupling geometries on the spin-independent total charge currents and the spin current are explored in Fig. 5(a1), (a2), (b1) and (b2). Both the spin-up and spin-down components of the currents, $I_{\alpha\hat{n}_\alpha;+}(t)$ and $I_{\alpha\hat{n}_\alpha;-}(t)$, play a role in the time evolution. When the magnitude of $I_{\alpha\hat{n}_\alpha;-}(t)$ in the intermediate times is comparable with that of $I_{\alpha\hat{n}_\alpha;+}(t)$, the effect of smaller Γ_α leading to a slower approach to the steady state becomes more obvious. By the effective configuration for the spin-down currents, the spin-down currents on the left side in the intermediate times have higher magnitudes than those on the right due to the difference in the chemical potentials. Thus the slower process for smaller coupling is more clearly observed in Fig. 5 (a1) and (b1) (the slowest processes are still given by the smallest Γ_L here, see the blue dashed lines). This is less obvious in Fig. 5 (a2) and (b2) (see the magnitudes in the inset of (b2)).

The effects of different φ_+ 's away from the optimal value on $I_\alpha(t)$ and $\mathbf{I}_\alpha^S(t)$ are studied in Fig. 5(c1), (c2), (d1) and (d2), by keeping φ_- satisfying Eq. (44c). Since $I_{\alpha\hat{n}_\alpha;-}(t)$ has been fixed, different results for $I_\alpha(t)$ and $\mathbf{I}_\alpha^S(t)$ solely come from different behaviors of $I_{\alpha\hat{n}_\alpha;+}(t)$. Similarly, the different values of φ_+ have little effects on the times for these currents to reach their steady-state values. In contrast, they strongly affect the magnitudes of these currents over the time.

B. Dynamics of spin currents

In the last subsection, we have concentrated on the dynamics under the conditions of reaching fully polarized currents in the steady-state limit. In general when the system deviates from these conditions, both the spin-up and the spin-down components of the currents are nonzero and full spin-polarized currents are not attained. In this case, instead of studying separately the currents for spin up and spin down in some specific direction, it is more interesting to simply focus on the spin currents $\mathbf{I}_\alpha^S(t)$.

1. Spin currents due to SOI without the magnetic flux

We first consider the situation with no applied magnetic flux, namely, $\phi = 0$. The effective fluxes are then given by $\varphi_\pm = \pm\psi_{\text{so}}$. In this case, Eq. (42) becomes (see

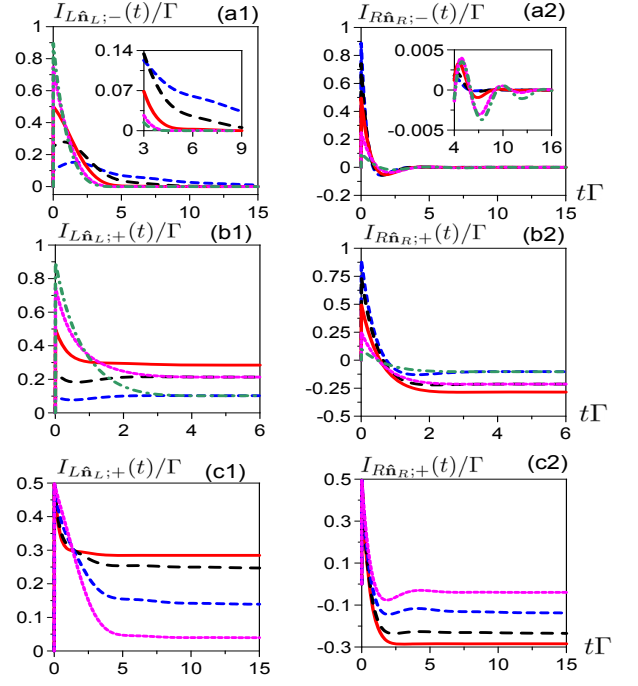


FIG. 4: (color online) Time evolutions of the currents $I_{\alpha\hat{n}_\alpha;-}(t)$ and $I_{\alpha\hat{n}_\alpha;+}(t)$ under the conditions of full spin polarizations. In (a1),(a2),(b1),(b2), the blue dashed lines are for $(\Gamma_L, \Gamma_R) = (0.1, 0.9)\Gamma$, the black long-dashed lines are for $(\Gamma_L, \Gamma_R) = (0.25, 0.75)\Gamma$, the red solid lines are for $(\Gamma_L, \Gamma_R) = (0.5, 0.5)\Gamma$, the magenta short-dashed lines are for $(\Gamma_L, \Gamma_R) = (0.75, 0.25)\Gamma$ and the green dash-dot lines are for $(\Gamma_L, \Gamma_R) = (0.9, 0.1)\Gamma$. In plots (a1) and (a2), $I_{L\hat{n}_L;-}(t)$ and $I_{R\hat{n}_R;-}(t)$ are shown for various coupling geometries respectively. The plots (b1) and (b2) respectively are for $I_{L\hat{n}_L;+}(t)$ and $I_{R\hat{n}_R;+}(t)$ at the optimal point $\varphi_+ = 2\pi$. In (c1) and (c2), the time evolutions of the currents $I_{L\hat{n}_L;+}(t)$ and $I_{R\hat{n}_R;+}(t)$ are plotted for various φ_+ with a fixed coupling geometry $(\Gamma_L, \Gamma_R) = (0.5, 0.5)\Gamma$. The red solid lines are with $\varphi_+ = 2\pi$, black long-dashed lines are with $\varphi_+ = 2\frac{1}{4}\pi$, blue dashed lines are with $\varphi_+ = 2\frac{1}{2}\pi$ and the magenta short-dashed lines are with $\varphi_+ = 2\frac{3}{4}\pi$. In all plots, we have set $\delta E = 0$, as one of the polarization conditions, and a bias $\mu_L = -\mu_R = 1.25\Gamma$ is applied at temperature $k_B T = \Gamma/20$. This set of bias and temperature is also assumed in the following figures. The instantaneous rising of the currents to finite values immediately after $t = 0$ in these plots is a direct consequence of the wide-band limit.⁷⁶

Appendix D for details)

$$\begin{aligned} \mathbf{I}_\alpha^S(t) \cdot \hat{\mathbf{n}}_\alpha &= -2\Gamma_L\Gamma_R\delta E \sin(\psi_{\text{so}}) \times \\ &\int \frac{d\omega}{2\pi} \left\{ f_-(\omega) \frac{1}{|\Gamma\psi_{\text{so}}|^2} \frac{d}{dt} [|u_p(t, \omega)|^2] \right. \\ &\left. \mp f_+(\omega) \left[\text{Re} \left(\frac{u_0^*(t, \omega) u_p(t, \omega)}{\Gamma\psi_{\text{so}}} \right) - \Gamma | \frac{u_p(t, \omega)}{\Gamma\psi_{\text{so}}} |^2 \right] \right\}. \end{aligned} \quad (77)$$

where $f_\pm(\omega) = f_L(\omega) \pm f_R(\omega)$ and $u_{0,p}(t, \omega) = \int_0^t d\tau e^{i\omega\tau} u_{0,p}(\psi_{\text{so}}, \tau)$. The upper sign is for $\alpha = L$ and

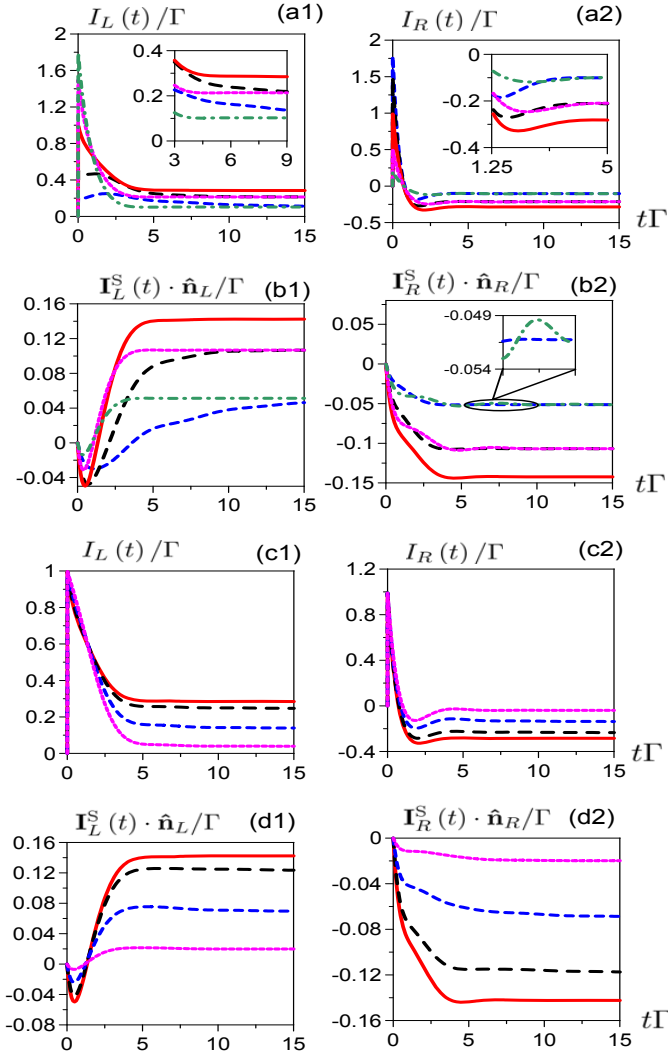


FIG. 5: (color online) The time evolution of the spin-independent total currents and the spin currents on the two electrodes are presented. Since the vector part of the spin current is not changing in time, it's sufficient to present its component along the characteristic direction, namely, $\mathbf{I}_\alpha^S(t) \cdot \hat{\mathbf{n}}_\alpha = (I_{\alpha\hat{\mathbf{n}}_\alpha;+}(t) - I_{\alpha\hat{\mathbf{n}}_\alpha;-}(t))/2$. These currents with various coupling geometries are displayed in (a1),(a2),(b1) and (b2) using the same parameters as in Fig. 4. Plots (c1), (c2), (d1) and (d2) show the results for the spin-independent total currents and the spin currents from various φ_+ 's, as used in Fig. 4(c1,c2).

the lower sign is for $\alpha = R$. Equation (77) shows that if we set $\delta E = 0$, then the spin currents remain zero for all time t . To generate a non-vanishing spin current, one has to lift up the degeneracy. From Eq. (D6), one finds that $\delta E = 0$ leads to $I_Q^0(\psi_{\text{so}}, t) = I_Q^0(-\psi_{\text{so}}, t)$ and $I_{\text{net}}^0(\psi_{\text{so}}, t) = I_{\text{net}}^0(-\psi_{\text{so}}, t)$ and phase rigidity is kept for the underlying spinless system throughout the time. Therefore, generating spin currents by lifting up the degeneracy is equivalent to the temporary breaking of phase rigidity in the spinless DQD interferometer, as

pointed out in Ref. [69]. Besides the energy splitting, Eq. (77) also explicitly reveals the necessity of the presence of SOI for the existence of the spin currents, through the term $\sin(\psi_{\text{so}})$. When SOI is absent, $\psi_{\text{so}} = 0$, then $\sin(\psi_{\text{so}}) = 0$, directly leading to $\mathbf{I}_\alpha^S(t) = 0$. Substituting Eq. (58) with $\varphi_\pm = \pm\psi_{\text{so}}$ into Eq. (77), the spin currents $\mathbf{I}_\alpha^S(t)$ will approach zero at long times. The non-vanishing spin currents can thus only be sustained transiently.

The above discussions show that the magnitudes of the transient spin currents are mainly determined by δE and $\sin(\psi_{\text{so}})$. In Fig. 6 (a1, a2), we study the effects of various δE 's on the time evolutions of the spin currents. The results show that splitting the degeneracy generally enhances the transient spin flow (compare the curves for smaller and bigger δE), as indicated by Eq. (77). Since bigger δE also implies faster relaxation, we observe a shorter span of nonzero spin flow with bigger energy splitting. The dependencies of the spin currents on SOI, through the SOI-induced phase ψ_{so} , are presented in Fig. 6 (b1, b2). The transient magnitudes increase with increasing values of $\sin(\psi_{\text{so}})$.

In parallel we also show the corresponding results for the spin-independent total charge currents for various δE 's in Fig. 7 (a1,a2) and for various ψ_{so} 's in Fig. 7 (b1,b2). Since the terms of Eqs. (D2,D3) that are even in the effective flux φ are proportional to δE^2 , the overall enhancement of the total current magnitudes with increasing δE is also observed in Fig. 7 (a1,a2). The dependence of the total current on ψ_{so} is different from the pattern dominated by $\sin\psi_{\text{so}}$ as the spin current in Fig. 6. The total charge currents generally persist to nonzero values, due to the finite bias voltage, as determined by Eq. (59).

2. Spin currents due to SOI with the magnetic flux

The above discussions have shown that it is not possible to generate spin currents at degeneracy purely by the act of SOI. Even when the degeneracy between the on-site energies of the DQD is lifted up, the spin currents only survive transiently. The magnetic flux is thus indispensable to sustain non-vanishing spin currents in the long time limit.

The versatility of the combination of the AB effect and the SOI for attaining various spin currents is demonstrated in Fig. 8 for both $\delta E = 0$ and $\delta E \neq 0$. The values of ϕ are so chosen that one can attain various distinct results for the spin current. In Fig. 8(a1,a2), we illustrate that at $\delta E = 0$, spin currents can be generated and sustained in the steady states by simultaneously setting $\phi \neq 0$ and $\sin(\psi_{\text{so}}) \neq 0$. The solution Eq. (42) implies that one can reverse the sign of the spin currents by just adjusting the flux ϕ , without altering the SOI parameters leading to the changes of $\hat{\mathbf{n}}_\alpha$ and ψ_{so} . At degeneracy, the currents $I_\alpha^0(\varphi_\pm, t)$ for the effective spinless system depend on the effective flux φ_\pm only through the term $\cos\varphi_\pm$

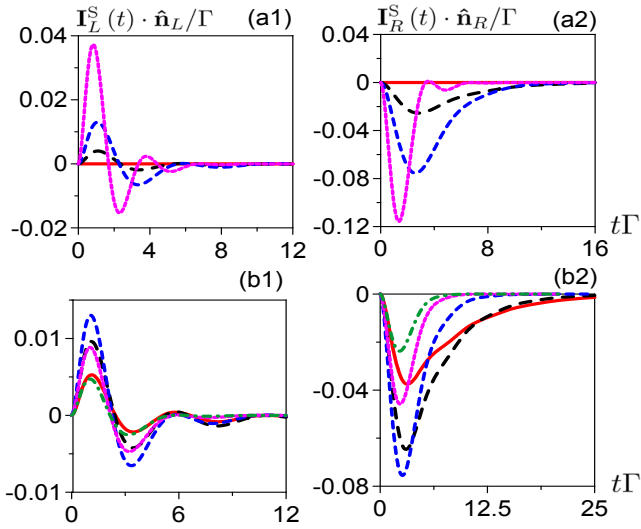


FIG. 6: (color online) Time evolutions of the spin currents. The couplings are set to $\Gamma_L = \Gamma_R = \Gamma/2$ here and also in the following Figs. 7-9. In plots (a1) and (a2) all curves are with $\psi_{so} = 0.5\pi$. The red solid lines are for $\delta E = 0$, the black long-dashed lines are for $\delta E = 0.15\Gamma$, the blue dashed lines are for $\delta E = 0.5\Gamma$ and the magenta short-dashed lines are for $\delta E = 2\Gamma$. In plots (b1) and (b2) we fix $\delta E = 0.5\Gamma$. The red solid lines are for $\psi_{so} = 0.125\pi$, the black long-dashed lines are for $\psi_{so} = 0.25\pi$, the blue dashed lines are for $\psi_{so} = 0.5\pi$, the magenta short-dashed lines are for $\psi_{so} = 0.75\pi$ and the green dash-dot lines are for $\psi_{so} = 0.875\pi$.

(see appendix D). Therefore, for all times t , the sign of $\mathbf{I}_\alpha^S(t) \cdot \hat{\mathbf{n}}_\alpha|_{\phi=n\pi+\Delta\phi}$ and that of $\mathbf{I}_\alpha^S(t) \cdot \hat{\mathbf{n}}_\alpha|_{\phi=n\pi-\Delta\phi}$, for n being an arbitrary integer and $\Delta\phi$ being nonzero, are opposite to each other, as indicated in Fig. 8(a1,a2). By lifting up the degeneracy, the dependence of $I_\alpha^0(\varphi_\pm, t)$ on φ_\pm appears from both of the terms $\cos\varphi_\pm$ and $\sin\varphi_\pm$. As a result, the spin currents with $\delta E \neq 0$ are not perfectly antisymmetric with respect to $\phi = n\pi$, as shown by Fig. 8 (b1,b2). In contrast to the high sensitivity of the spin currents to the variation in the magnetic flux given nonzero SOI, the total currents are not obviously affected by different choices of ϕ , as shown in Fig. 9.

C. Deduction of the spin-resolved currents from the spin-independent total charge current

In section IV B, we have discussed how one can extract the values of ψ_{so} and ϕ at given electric and magnetic fields. With this knowledge in mind, by applying similar procedures, we can also obtain the magnitude of the spin current, $\mathbf{I}_\alpha^S(t) \cdot \hat{\mathbf{n}}_\alpha$, from the values of the spin-independent total charge current. Explicitly, the spin-independent total charge current, Eq. (39), at given electric and magnetic fields is

$$I_\alpha(\phi, \psi_{so}, t) = I_\alpha^0(\varphi_+, t) + I_\alpha^0(\varphi_-, t). \quad (78)$$

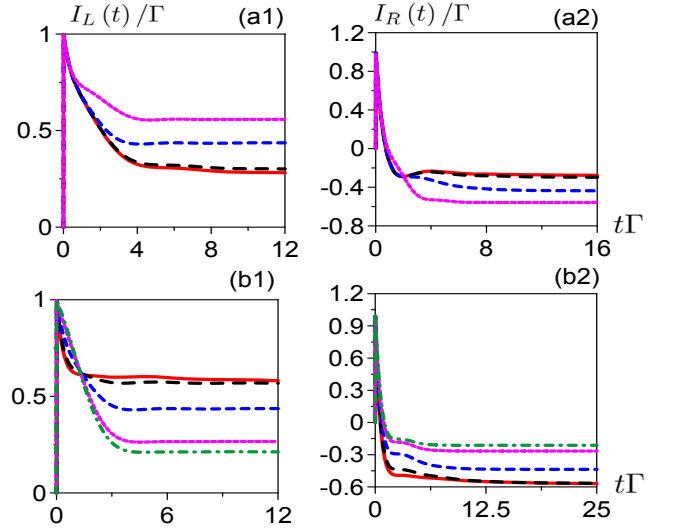


FIG. 7: (color online) Time evolutions of the total currents. The parameters used here in (a1) and (a2) are the same as those in the plots (a1,a2) of Fig. 6. The parameters used here in (b1) and (b2) are the same as those in the plots (b1,b2) of Fig. 6.

From Eq. (D5) with Eqs. (D2, D3), the current on lead α for the effective spinless DQD system with flux φ can be split into two terms,

$$I_\alpha^0(\varphi, t) = \bar{I}_\alpha^0(\varphi, t) + \delta E \sin(\varphi) \bar{I}_\alpha^\gamma(\varphi, t), \quad (79a)$$

where $\bar{I}_\alpha^0(\varphi, t)$ and $\bar{I}_\alpha^\gamma(\varphi, t)$ satisfy,

$$\bar{I}_\alpha^0(\varphi, t) = \bar{I}_\alpha^0(-\varphi, t), \quad \bar{I}_\alpha^\gamma(\varphi, t) = \bar{I}_\alpha^\gamma(-\varphi, t). \quad (79b)$$

Setting zero magnetic field $\phi = 0$ in Eq. (78) with the property given by Eq. (79), the dependence of the total charge current on ψ_{so} becomes

$$I_\alpha(\phi = 0, \psi_{so}, t) = 2\bar{I}_\alpha^0(\psi_{so}, t). \quad (80)$$

The dependence of $\bar{I}_\alpha^0(\psi_{so}, t)$ on various ψ_{so} 's can thus be found from the total current $I_\alpha(\phi = 0, \psi_{so}, t)$ under different applied electric fields with zero magnetic flux. The dependence of $\bar{I}_\alpha^\gamma(\varphi, t)$ on φ can be found through the following approach. By fixing the electric field at $\psi_{so} = 2n\pi$, this part of the current is related to the total current and to the part that is already known, $\bar{I}_\alpha^0(\varphi, t)$, via the relation

$$2\delta E \sin(\phi) \bar{I}_\alpha^\gamma(\phi, t) = I_\alpha(\phi, \psi_{so} = 2n\pi, t) - 2\bar{I}_\alpha^0(\phi, t). \quad (81)$$

The values of $\bar{I}_\alpha^\gamma(\phi, t)$ for different ϕ 's can thus be deduced from the total current and $\bar{I}_\alpha^0(\phi, t)$ by applying the corresponding magnetic fields. Knowing $I_\alpha^0(\varphi, t)$ at various effective fluxes φ , one can deduce the spin-resolved current by the virtue of Eq. (37).

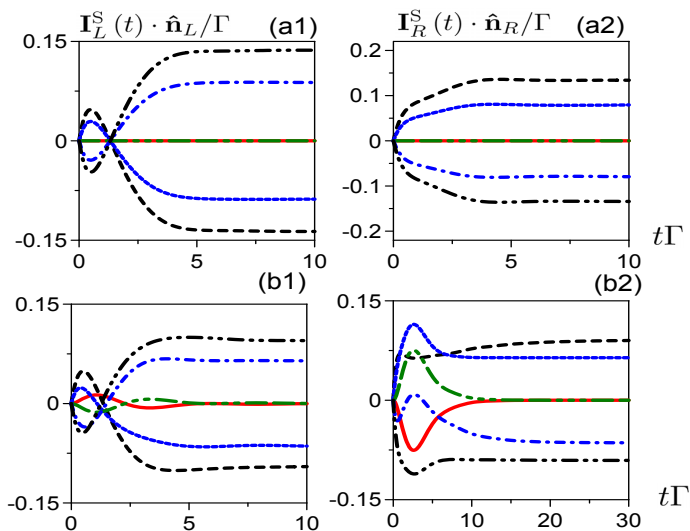


FIG. 8: (color online) Various magnetic flux values are tested for fixed SOI strength. In all plots we let $\psi_{\text{so}} = 0.5\pi$. In plots (a1) and (a2), we set $\delta E = 0$. The red solid lines for $\phi = 0$ and the dark green dash-dash-dot-dot-dot lines for $\phi = \pi$ are overlapped. The black-dashed lines for $\phi = 0.4\pi$ and the black dash-dot-dot lines for $\phi = 1.6\pi$ differ by a sign. The blue short-dashed lines for $\phi = 0.8\pi$ and the blue dash-dot lines for $\phi = 1.2\pi$ also differ by a sign. In plots (b1) and (b2), the degeneracy is lifted as $\delta E = 0.5\Gamma$ and the same choices of ϕ used in (a1) and (a2) are used also here.

VI. SUMMARY AND CONCLUSION

In this work, we have applied our previously developed non-equilibrium approach to explore the real-time dynamics of spin-dependent electron transport through a DQD AB interferometer with SOI. We have obtained the real-time evolution of the spin-resolved currents, Eq. (43), and the subsequent spin currents Eq. (42). These expressions fully describe the dynamical evolution of the spin-polarizations in the electron transport from initially completely unpolarized interferometers. The currents are expressed in terms of the currents for the spinless DQD AB interferometer, Eq. (55), through the identification Eq. (37). Such connections explicitly reveal that it is the difference between the effective fluxes, $\varphi_{\pm} = \phi \pm \psi_{\text{so}}$, caused by the SOI, that gives rise to the spin-polarizations. Importantly, it is also manifested that spin-polarizations of currents in each lead are only developed along their characteristic directions throughout all times. These characteristic directions, $\hat{\mathbf{n}}_L$ and $\hat{\mathbf{n}}_R$, are fully determined from the settings of SOI, regardless of the applied magnetic flux. Using these expressions, we have particularly investigated the real-time evolution of the currents towards fully spin-polarized transport. We have also explored the interplay between the SOI and AB interferences in the dynamics of spin flows.

The spin-resolved transport dynamics are described by the time evolution of the spin-up and spin-down cur-

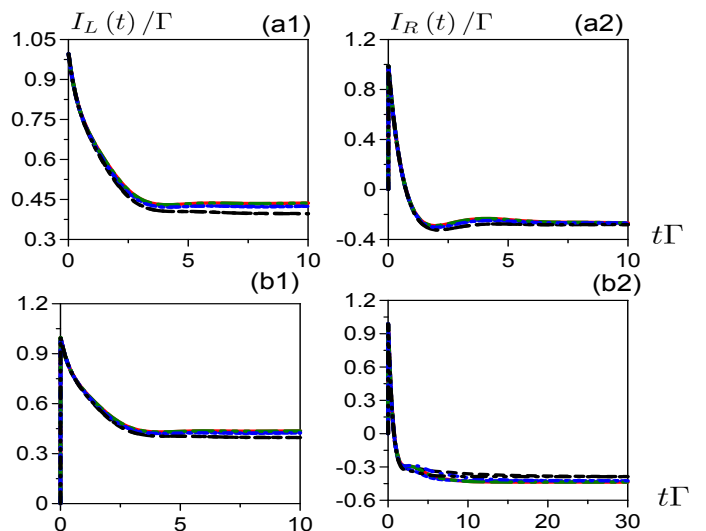


FIG. 9: (color online) Time evolutions of the total currents. The parameters used here in (a1) and (a2) are the same as those in the plots (a1,a2) of Fig. 8. The parameters used here in (b1) and (b2) are the same as those in the plots (b1,b2) of Fig. 8.

rents along the characteristic directions in each of the two leads. Full spin-polarization is a process in which the spin-down currents eventually decay to zero while the spin-up currents remain nonzero. When the conditions for full spin-polarization (in the “up”-direction) are fulfilled, we find that the spin-down currents in each of the leads can be identified with the currents through a spinless system described in Fig. 2(a). This consists of two separate systems, each of which is an effective single level dot coupled to an electron reservoir. Therefore, how fast the current for each of these separate systems decays to zero is determined by the coupling to that electrode. On the other hand, the currents for spin-up electrons in each of the leads are influenced by parameters from both of the leads. In the wide-band limit, the couplings to the leads are simply given by the constants Γ_L and Γ_R . The time for the currents to reach their steady-state values are characterized by the inverse of the total coupling $\Gamma^{-1} = (\Gamma_L + \Gamma_R)^{-1}$. Since $\Gamma > \Gamma_{\alpha}$, for $\alpha = L, R$, the spin-down currents decay to zero slower than the spin-up currents arrive to their steady-state values. The dependence of the spin polarization processes on the SOI parameters appears via the SOI-induced phase ψ_{so} in the effective flux $\varphi_{+} = \phi + \psi_{\text{so}}$. Given that the conditions in Eq. (44) are satisfied, different SOI parameters and magnetic fluxes only influence the time evolution of the spin-up currents in each of the leads. The choices of the SOI parameters and ϕ under full polarization conditions mainly affect the magnitude of the steady-state spin-polarized currents. They do not have an obvious influence on the time scale for the spin-up currents to reach steady state.

The realization of full spin polarization has received

considerable attention, as it supplies spin-polarized electron sources and allows the manipulation of flying spin qubits. Therefore how fast spin-polarization can be arrived is important. In the present system, the spin-filtering function has been associated with the flying qubit application. Our results show that when the full spin-polarization conditions are implemented, the dynamical process for the currents of one spin-component to completely vanish is also fixed. The only tunable parameter affecting the speed of this process is the tunnel couplings to the left and the right leads. Henceforth, to increase the pace toward fully spin-polarized transport, one has to use stronger couplings Γ_L and Γ_R .

The generation of full spin-polarized currents requires both the magnetic flux and the SOI. By setting the flux equal to zero, we found that SOI alone cannot support any spin flow to the steady-state limit. This is due to the phase rigidity for the effective spinless system as a two-terminal setup. Breaking phase rigidity by lifting up the degeneracy between the on-site energies of the DQD can lead to transient spin currents. With a finite magnetic flux, the combined charge and spin interference effects are crucial for sustaining of spin polarization in the steady-state. The combined effect of the AB phase and of the SOI-induced phase allows for the modulation of the polarization direction by the magnetic flux.

An ongoing experimental issue concerns the possibility to detect spin-polarized electrical currents using only electrical means.⁷⁷⁻⁸⁰ Spin-independent transport quantities, like charge currents, are readily measurable in experiments. We have shown how one can extract information on the spin-resolved currents in this system from measurements of the total charge currents. Such measurements can thus be used for testing the properties of the spin-resolved transport. Modulating electron transport via interference in ring-like structures with the AB effect^{81,82} and spin interference¹²⁻¹⁴ are of much experimental interest. The analysis of the time evolution of spin-resolved transport for this DQD interferometer could add a momentum to this progressing research direction.

Acknowledgments

Work at NCKU is partially supported by the National Science Council (NSC) of the ROC, under Contract No. NSC102-2112-M-006-016-MY3, by the Headquarters of University Advancement at the National Cheng Kung University, which is sponsored by the Ministry of Education, Taiwan, ROC and from the National Center for Theoretical Science of NSC and the High Performance Computing Facility in the National Cheng Kung University. Work at Ben Gurion University was supported by grants from the Israel Science Foundation (ISF) and from the U.S.-Israel Binational Science Foundation (BSF).

Appendix A: Determination of the SOI induced phase and the characteristic directions from the bonding geometry and SOI strength

In this appendix, we replicate the relation connecting the bonding geometry of the present system and the SOI strength to the SOI-induced phase and characteristic directions from Ref. [41]. The bonding geometry is characterized by the bonding angle β , see Fig. 1. We consider here only Rashba SOI by setting $\alpha_D = 0$ in Eq. (24).

We assume that there is only one localized charge state in each of the lead which is connected to the DQD system such that we only have one SOI-induced phase. The positions of the left connecting site, the first dot, the right connecting site and the second dot are respectively denoted by \mathbf{r}_L , \mathbf{r}_1 , \mathbf{r}_R and \mathbf{r}_2 . The connecting side on the left electrode sits at the origin of the coordinates. The coordinates of the four positions are given by $\mathbf{r}_L = 0\hat{\mathbf{x}} + 0\hat{\mathbf{y}}$, $\mathbf{r}_1 = L(\cos\beta\hat{\mathbf{x}} + \sin\beta\hat{\mathbf{y}})$, $\mathbf{r}_2 = L(\cos\beta\hat{\mathbf{x}} - \sin\beta\hat{\mathbf{y}})$ and $\mathbf{r}_R = 2L\cos\beta\hat{\mathbf{x}} + 0\hat{\mathbf{y}}$, where L is the bond length. Under this condition, the spin rotations from Eq. (24) for each section become

$$\begin{aligned} U^{L1} &= \cos(\alpha_R) + i\sin(\alpha_R)[\sin\beta\sigma_x - \cos\beta\sigma_y], \\ U^{1R} &= \cos(\alpha_R) + i\sin(\alpha_R)[- \sin\beta\sigma_x - \cos\beta\sigma_y], \\ U^{R2} &= \cos(\alpha_R) + i\sin(\alpha_R)[- \sin\beta\sigma_x + \cos\beta\sigma_y], \\ U^{2L} &= \cos(\alpha_R) + i\sin(\alpha_R)[\sin\beta\sigma_x + \cos\beta\sigma_y]. \end{aligned}$$

Rewriting the formal expression, Eq. (25), as $U^x = \exp(-i\psi_{\text{so}}\hat{\mathbf{n}}_x \cdot \boldsymbol{\sigma})$ for $x = L, 1, R$ and 2 , the choice of fixing ψ_{so} to be positive has led to

$$\begin{aligned} \cos\psi_{\text{so}} &= 1 - 2\sin^4(\alpha_R)\sin^2(2\beta), \\ \sin\psi_{\text{so}} &= 2\sin^2(\alpha_R)\sin(2\beta)\sqrt{1 - \sin^4(\alpha_R)\sin^2(2\beta)}. \end{aligned} \quad (\text{A1})$$

In Ref. [41], the authors diagonalized the quantities, $\mathbf{W}\mathbf{W}^\dagger$ and $\mathbf{W}^\dagger\mathbf{W}$, where $\mathbf{W} = \gamma_b U_b + \gamma_c U_c$ (using the notations in that paper), in which $\gamma_{b,c}$ are some real scalar coefficients relating to couplings to the leads. The unitary spin rotations are identified to be $U_b = U^{L1}U^{1R}$ and $U_c = U^{L2}U^{2R}$. The spin rotations around the loop commute with these quantities, namely, $[\mathbf{W}\mathbf{W}^\dagger, U^L] = 0$ and $[\mathbf{W}^\dagger\mathbf{W}, U^R] = 0$. Therefore the eigenstates of $\mathbf{W}\mathbf{W}^\dagger$ ($\mathbf{W}^\dagger\mathbf{W}$) are also those of U^L (U^R) as needed here.

The eigenvectors of U^L are $|\hat{\mathbf{n}}_L; \pm\rangle$ corresponding to eigenvalues $e^{\mp i\psi_{\text{so}}}$. The characteristic direction $\hat{\mathbf{n}}_L$ is given by

$$\begin{aligned} \hat{\mathbf{n}}_L \cdot \hat{\mathbf{x}} &= -\frac{2\cos(\alpha_R)\sin(\alpha_R)\cos(\beta)}{\sqrt{1 - \sin^4(\alpha_R)\sin^2(2\beta)}}, \\ \hat{\mathbf{n}}_L \cdot \hat{\mathbf{y}} &= 0, \\ \hat{\mathbf{n}}_L \cdot \hat{\mathbf{z}} &= \frac{\sin^2(\alpha_R)\cos(2\beta) - \cos^2(\alpha_R)}{\sqrt{1 - \sin^4(\alpha_R)\sin^2(2\beta)}}. \end{aligned} \quad (\text{A2a})$$

The eigenvectors for U^R are $|\hat{\mathbf{n}}_R; \pm\rangle$ with

$$\begin{aligned}\hat{\mathbf{n}}_R \cdot \hat{\mathbf{x}} &= -\hat{\mathbf{n}}_L \cdot \hat{\mathbf{x}}, \\ \hat{\mathbf{n}}_R \cdot \hat{\mathbf{y}} &= 0, \\ \hat{\mathbf{n}}_R \cdot \hat{\mathbf{z}} &= \hat{\mathbf{n}}_L \cdot \hat{\mathbf{z}}.\end{aligned}\quad (\text{A2b})$$

Appendix B: The spinless DQD AB interferometer for arbitrary level-broadening functions

In our previous work,⁶⁹ we have presented the specific expressions for the self-energy, Eq. (12a) and Green functions Eqs. (13a, 13b), in the wide-band limit for the spinless DQD AB interferometer. To compare the general expressions, shown in section III D, before the wide-band limit is assumed, here we present explicitly these basic quantities for such a spinless system with arbitrary form of Eq. (12b). We have shown in our previous work that the free gauge that appears in the Green functions will

be cancelled in the expressions for the currents, using the solutions in the wide-band limit. Here we prove this is also held for an arbitrary level-broadening function.

The Hamiltonian for the spinless DQD AB interferometer is given by $\mathcal{H} = \mathcal{H}_S + \mathcal{H}_E + \mathcal{H}_T$, where the Hamiltonian for the DQD is $\mathcal{H}_S = \sum_{i=1}^2 E_i a_i^\dagger a_i$, the Hamiltonian for the reservoirs is $\mathcal{H}_E = \sum_{\alpha\mathbf{k}} \epsilon_{\alpha\mathbf{k}} c_{\alpha\mathbf{k}}^\dagger c_{\alpha\mathbf{k}}$ and the tunneling between them is $\mathcal{H}_T = \sum_{i\alpha\mathbf{k}} [V_{i\alpha\mathbf{k}} a_i^\dagger c_{\alpha\mathbf{k}} + \text{h.c.}]$. The AB effect is embedded in the tunneling amplitude as described by Eq. (23). The self-energies induced by each lead, given by Eq. (12a), become, $[\mathbf{g}_\alpha(\tau)]_{ij} = [\bar{\mathbf{g}}_\alpha(\tau)]_{ij} e^{i(\phi_{i\alpha} - \phi_{\alpha j})}$ and $\tilde{\mathbf{g}}_\alpha(\tau) = \bar{\tilde{\mathbf{g}}}_\alpha(\tau) e^{i(\phi_{i\alpha} - \phi_{\alpha j})}$, where $\bar{\mathbf{g}}_\alpha(\tau) = \int \frac{d\omega}{2\pi} f_\alpha(\omega) \mathbf{\Gamma}^\alpha(\omega) e^{-i\omega\tau}$ and $\bar{\tilde{\mathbf{g}}}_\alpha(\tau) = \int \frac{d\omega}{2\pi} \mathbf{\Gamma}^\alpha(\omega) e^{-i\omega\tau}$, with $[\bar{\mathbf{\Gamma}}^\alpha(\omega)]_{ij} = 2\pi \sum_{k \in \alpha} \bar{V}_{i\alpha k} \bar{V}_{j\alpha k}^* \delta(\omega - \epsilon_{\alpha k})$ for $\alpha \in \{L, R\}$ and $i, j \in \{1, 2\}$. The corresponding 2×2 matrix of the total self-energy function, $\mathbf{g}(\tau) = \sum_\alpha \mathbf{g}_\alpha(\tau)$, is

$$\mathbf{g}(\tau) = \begin{pmatrix} [\bar{\mathbf{g}}_L(\tau)]_{11} + [\bar{\mathbf{g}}_R(\tau)]_{11} & e^{i\chi} ([\bar{\mathbf{g}}_L(\tau)]_{12} e^{i\phi/2} + [\bar{\mathbf{g}}_R(\tau)]_{12} e^{-i\phi/2}) \\ e^{-i\chi} ([\bar{\mathbf{g}}_L(\tau)]_{21} e^{-i\phi/2} + [\bar{\mathbf{g}}_R(\tau)]_{21} e^{i\phi/2}) & [\bar{\mathbf{g}}_L(\tau)]_{22} + [\bar{\mathbf{g}}_R(\tau)]_{22} \end{pmatrix}, \quad (\text{B1})$$

where $\chi = (\phi_L + \phi_R)/2$ is an arbitrary gauge phase. Clearly, there is a one-to-one correspondence between Eq. (B1) and Eq. (54), with $\chi \leftrightarrow \chi_\pm$ and $\phi \leftrightarrow \varphi_\pm$. The Green functions, satisfying Eqs. (13a, 13b), with the self-energies given above, are also in a one-to-one correspondence with those prescribed by Eqs. (53b, 53c). The current on lead α , given by Eq. (20), here reads

$$\begin{aligned}I_\alpha(t) &= 2e \text{ReTr} \int_0^t d\tau (\tilde{\mathbf{g}}_\alpha(t-\tau) \bar{\mathbf{u}}(\tau) - \mathbf{g}_\alpha(t-\tau) \mathbf{v}(\tau)), \\ & \quad (\text{B2})\end{aligned}$$

with an obvious correspondence with Eq. (55) is seen.

Using the formal solutions of $\mathbf{u}(\tau)$ and $\mathbf{v}(\tau)$, we prove in what follows that $I_\alpha(t)$ is independent of χ . The formal solution of $\mathbf{u}(\tau)$ is given by

$$\mathbf{u}(\tau) = \int_{-\infty+i\omega_c}^{+\infty+i\omega_c} \frac{d\omega}{2\pi} e^{-i\omega\tau} \tilde{\mathbf{u}}(\omega) \quad (\text{B3a})$$

with ω_c being some arbitrary positive number, where

$$\tilde{\mathbf{u}}(\omega) = i(\omega \mathbf{1} - \mathbf{E} - \mathbf{\Sigma}(\omega))^{-1}$$

in which \mathbf{E} is the 2×2 diagonal energy matrix for the DQD. Here $\mathbf{\Sigma}(\omega) = \sum_{\alpha=L,R} \mathbf{\Sigma}_\alpha(\omega)$ with $[\mathbf{\Sigma}_\alpha(\omega)]_{ij} = [\bar{\mathbf{\Sigma}}_\alpha(\omega)]_{ij} e^{i(\phi_{i\alpha} - \phi_{\alpha j})}$ and $\bar{\mathbf{\Sigma}}_\alpha(\omega) = \int \frac{d\nu}{2\pi} \frac{\bar{\Gamma}^\alpha(\nu)}{\omega - \nu}$ is the self-energy induced by coupling to lead α in the frequency

domain. Explicitly,

$$\tilde{\mathbf{u}}(\omega) = \frac{i}{D(\omega)} \begin{pmatrix} \omega - E_2 - \bar{\Sigma}_{22}(\omega) & \sum_\alpha \bar{\Sigma}_{\alpha 12}(\omega) e^{i\phi_\alpha} \\ \sum_\alpha \bar{\Sigma}_{\alpha 21}(\omega) e^{-i\phi_\alpha} & \omega - E_1 - \bar{\Sigma}_{11}(\omega) \end{pmatrix}, \quad (\text{B3b})$$

with

$$\begin{aligned}D(\omega) &= \prod_{i=1}^2 (\omega - E_i - \bar{\Sigma}_{ii}(\omega)) - \sum_{\alpha=L,R} |\bar{\Sigma}_{\alpha 12}(\omega)|^2 \\ &\quad - 2\text{Re} [\bar{\Sigma}_{L12}(\omega) \bar{\Sigma}_{R21}(\omega) e^{i\phi}], \quad (\text{B3c})\end{aligned}$$

being the determinant of the matrix $(\omega \mathbf{1} - \mathbf{E} - \mathbf{\Sigma}(\omega))$. Here $D(\omega)$ is independent of χ . It is clear from Eq. (B3) that only the off-diagonal terms of $\mathbf{u}(\tau)$ depend on the gauge χ . Expanding the trace in Eq. (B2), the only terms that may depend on χ are $[\bar{\mathbf{g}}_\alpha(t-\tau)]_{12} [\bar{\mathbf{u}}(\tau)]_{21} - [\mathbf{g}_\alpha(t-\tau)]_{12} [\mathbf{v}(\tau)]_{21}$ and $[\bar{\mathbf{g}}_\alpha(t-\tau)]_{21} [\bar{\mathbf{u}}(\tau)]_{12} - [\mathbf{g}_\alpha(t-\tau)]_{21} [\mathbf{v}(\tau)]_{12}$. Substitute the formal solution Eq. (B3a) with explicit dependencies on ϕ_α from Eq. (B3b) into these two terms, we find the dependence on χ in the Green functions exactly cancel that in $\mathbf{g}_\alpha(t-\tau)$ and $\bar{\mathbf{g}}_\alpha(t-\tau)$. This completes the proof that the current $I_\alpha(t)$ is independent of the gauge χ for arbitrary level-broadening functions. The same procedure can be straightforwardly repeated to prove that $I_\alpha^0(\varphi_\pm, t)$ is independent of χ_\pm .

Appendix C: The current formulae for a single level coupled to one and two electron reservoirs

In section V A, we have compared the spin-resolved currents through a DQD AB interferometer with SOI with the currents through a spinless single level coupled to electron reservoirs. Here we explicitly derive the expressions for the currents in these simple systems using the wide-band limit. This then verifies the above identifications explicitly.

1. The current through a spinless single level coupled to one lead

The total Hamiltonian for a spinless single level coupled to one electrode is given by $\mathcal{H} = \mathcal{H}_S + \mathcal{H}_E + \mathcal{H}_T$. Here $\mathcal{H}_S = \epsilon_0 a^\dagger a$ denotes the Hamiltonian of the spinless single-level system, $\mathcal{H}_E = \sum_k \epsilon_k c_k^\dagger c_k$ describes the single reservoir. The tunneling is given by $\mathcal{H}_T = \sum_k [V_{0k} a^\dagger c_k + \text{h.c.}]$. Using Eq. (13a) in the white-band limit, we have $u(\tau) = \exp(-i\epsilon_0\tau - \gamma t/2)$ where γ is the broadening due to coupling. Since the system is a single level, $u(\tau)$ is a scalar. The current is defined by $I(t) = -\frac{d}{dt} \sum_k \text{tr}_{\text{tot}}[c_k^\dagger c_k \rho_{\text{tot}}(t)]$. Substituting this solution into Eq. (20), we obtain the corresponding current,

$$I(t) = 4 \times \left(\frac{\gamma}{2}\right) \int \frac{d\omega}{2\pi} f(\omega) \frac{e^{-\gamma t/2} \left(\frac{\gamma}{2} \cos \omega t + \omega \sin \omega t\right) - \frac{\gamma}{2} e^{-\gamma t}}{\omega^2 + \left(\frac{\gamma}{2}\right)^2} \quad (\text{C1})$$

where $f(\omega)$ is the fermi function for that electron reservoir. Identifying $\frac{\gamma}{2}$ with Γ_α , Eq. (75) and Eq. (C1) are the same.

2. The current through a spinless single level coupled to two leads

For a spinless single level coupled to two electrodes, the Hamiltonian for the reservoirs becomes $\mathcal{H}_E =$

$\sum_{\alpha k} \epsilon_{\alpha k} c_{\alpha k}^\dagger c_{\alpha k}$ for $\alpha = L, R$. The tunneling is given by $\mathcal{H}_T = \sum_{\alpha k} [V_{\alpha k} a^\dagger c_{\alpha k} + \text{h.c.}]$. The corresponding Green function in the white-band limit is $u(\tau) = \exp(-i\epsilon_0\tau - \gamma_+\tau)$ where $\gamma_+ = (\gamma_L + \gamma_R)/2$. The current on lead α is defined by $I_\alpha(t) = -\frac{d}{dt} \sum_k \text{tr}_{\text{tot}}[c_{\alpha k}^\dagger c_{\alpha k} \rho_{\text{tot}}(t)]$. Consequently, from Eq. (20), this current reads

$$I_\alpha(t) = 2\gamma_\alpha \int \frac{d\omega}{2\pi} \left\{ f_\alpha(\omega) \frac{[\gamma_+ + (\omega \sin(\omega t) - \gamma_+ \cos(\omega t)) e^{-\gamma_+ t}]}{\omega^2 + \gamma_+^2} - \sum_{\alpha'=L,R} \frac{\gamma_{\alpha'}}{2} f_{\alpha'}(\omega) \frac{(1 + e^{-2\gamma_+ t} - 2 \cos(\omega t) e^{-\gamma_+ t})}{\omega^2 + \gamma_+^2} \right\}. \quad (\text{C2})$$

Setting the coupling to one of lead as zero, for example, $\gamma_R = 0$, and letting $\gamma_L = \gamma$, Eq. (C2) immediately reduces to Eq. (C1). Identification of Eq. (C2) with Eq. (76) is done via equating $\frac{\gamma_\alpha}{2}$ with Γ_α . Note that in both expressions Eqs. (C1, C2), we have set $\epsilon_0 = 0$ as an energy reference.

Appendix D: Derivation of Eq. (77)

By Eq. (37), the spin-resolved currents and consequently the spin currents can all be explicitly found by calculating the currents for the corresponding spinless DQD system with the effective flux φ_\pm . We have presented in our previous work⁶⁹ the results for the time evolution of the total occupation number in the DQD, $N_0(\varphi_\pm, t)$, and the transport current

$$I_{\text{net}}^0(\varphi_\pm, t) \equiv (I_L^0(\varphi_\pm, t) - I_R^0(\varphi_\pm, t))/2. \quad (\text{D1})$$

The total occupation number is given by Eq. (19) in Ref. [69]. Here we change ϕ to the effective flux φ_\pm and replicate

$$N_0(\varphi_\pm, t) = \int \frac{d\omega}{2\pi} f_+(\omega) \left\{ \Gamma \left[|u_0(t, \omega)|^2 + (\Gamma_{\varphi_\pm}^2 + 2\delta E^2) \left| \frac{u_p(t, \omega)}{\Gamma_{\varphi_\pm}} \right|^2 \right] - 2(\Gamma_{\varphi_\pm}^2 + \delta E^2) \text{Re} \left[\frac{u_0^*(t, \omega) u_p(t, \omega)}{\Gamma_{\varphi_\pm}} \right] \right\} + \int \frac{d\omega}{2\pi} f_-(\omega) \delta \Gamma \left\{ |u_0(t, \omega)|^2 + \left(\Gamma_{\varphi_\pm}^2 + 2\delta E^2 - (\Gamma^2 - \delta \Gamma^2) \frac{\delta E}{\delta \Gamma} \sin \varphi_\pm \right) \left| \frac{u_p(t, \omega)}{\Gamma_{\varphi_\pm}} \right|^2 - 2\Gamma \text{Re} \left[\frac{u_0^*(t, \omega) u_p(t, \omega)}{\Gamma_{\varphi_\pm}} \right] \right\}. \quad (\text{D2})$$

The transport current is found from Eq. (21) in Ref. [69]. Here it reads

$$\begin{aligned}
I_{\text{net}}^0(\varphi_{\pm}, t) = & \int \frac{d\omega}{2\pi} f_+(\omega) \left\{ \delta\Gamma \text{Re} \left(u_0(t, \omega) - \frac{\Gamma}{\Gamma_{\varphi_{\pm}}} u_p(t, \omega) \right) - \frac{\Gamma\delta\Gamma}{2} \left[2|u_0(t, \omega)|^2 + \left(\Gamma^2 \left[\cos^2 \frac{\varphi_{\pm}}{2} \cos \varphi_{\pm} \right. \right. \right. \\
& + \left. \left. \frac{\sin^2 \varphi_{\pm}}{2} + \frac{\delta E}{\delta\Gamma} \sin \varphi_{\pm} \right] - \delta\Gamma^2 \left[\sin^2 \frac{\varphi_{\pm}}{2} \cos \varphi_{\pm} - \frac{\sin^2 \varphi_{\pm}}{2} + \frac{\delta E}{\delta\Gamma} \sin \varphi_{\pm} \right] + \Gamma_{\varphi_{\pm}}^2 + \delta E^2 \right) \left| \frac{u_p(t, \omega)}{\Gamma_{\varphi_{\pm}}} \right|^2 \right\} \\
& + \left(\Gamma^2 \delta\Gamma \left(\cos^2 \frac{\varphi_{\pm}}{2} + 1 \right) + \delta\Gamma^3 \sin^2 \frac{\varphi_{\pm}}{2} + \frac{\Gamma^2 - \delta\Gamma^2}{2} \delta E \sin \varphi_{\pm} \right) \text{Re} \left[\frac{u_0^*(t, \omega) u_p(t, \omega)}{\Gamma_{\varphi_{\pm}}} \right] \\
& + \int \frac{d\omega}{2\pi} f_-(\omega) \left\{ \text{Re} \left(\Gamma u_0(t, \omega) - \frac{\Gamma_{\varphi_{\pm}}^2 + \delta E^2}{\Gamma_{\varphi_{\pm}}} u_p(t, \omega) \right) - \frac{\delta\Gamma^2 \left(\cos^2 \frac{\varphi_{\pm}}{2} + 1 \right) + \Gamma^2 \sin^2 \frac{\varphi_{\pm}}{2}}{2} |u_0(t, \omega)|^2 \right. \\
& - \frac{1}{2} \left(\left[\Gamma^2 \cos^2 \frac{\varphi_{\pm}}{2} - \delta\Gamma^2 \sin^2 \frac{\varphi_{\pm}}{2} - \delta E^2 \right] \delta\Gamma^2 \cos^2 \frac{\varphi_{\pm}}{2} - \left[\Gamma^2 \cos^2 \frac{\varphi_{\pm}}{2} - \delta\Gamma^2 \sin^2 \frac{\varphi_{\pm}}{2} + \delta E^2 \right] \Gamma^2 \sin^2 \frac{\varphi_{\pm}}{2} \right. \\
& \left. \left. + \delta\Gamma^2 \left(\Gamma_{\varphi_{\pm}}^2 + \Gamma^2 \sin^2 \varphi_{\pm} + 2\delta E^2 \right) \right) \left| \frac{u_p(t, \omega)}{\Gamma_{\varphi_{\pm}}} \right|^2 + 2\Gamma\delta\Gamma^2 \text{Re} \left[\frac{u_0^*(t, \omega) u_p(t, \omega)}{\Gamma_{\varphi_{\pm}}} \right] \right\}, \tag{D3}
\end{aligned}$$

In both Eqs. (D2, D3), $\delta\Gamma = \Gamma_L - \Gamma_R$ and $u_{0,p}(t, \omega) = \int_0^t d\tau e^{i\omega\tau} u_{0,p}(\varphi_{\pm}, \tau)$.

The individual currents on both of the leads can be obtained from these two quantities. By charge conservation, we have

$$\frac{d}{dt} N_0(\varphi_{\pm}, t) = I_L^0(\varphi_{\pm}, t) + I_R^0(\varphi_{\pm}, t). \tag{D4a}$$

We define half of the displacement current by

$$I_Q^0(\varphi_{\pm}, t) = \frac{1}{2} \frac{d}{dt} N_0(\varphi_{\pm}, t). \tag{D4b}$$

In terms of $I_Q^0(\varphi_{\pm}, t)$ and $I_{\text{net}}^0(\varphi_{\pm}, t)$, the individual currents are

$$I_L^0(\varphi_{\pm}, t) = I_Q^0(\varphi_{\pm}, t) + I_{\text{net}}^0(\varphi_{\pm}, t), \tag{D5a}$$

$$I_R^0(\varphi_{\pm}, t) = I_Q^0(\varphi_{\pm}, t) - I_{\text{net}}^0(\varphi_{\pm}, t). \tag{D5b}$$

Applying Eq. (37) to Eq. (42) with the above substitution, we find,

$$\begin{aligned}
\mathbf{I}_L^S(t) \cdot \hat{\mathbf{n}}_L = & \frac{1}{2} \times \\
& (I_Q^0(\varphi_+, t) - I_Q^0(\varphi_-, t) + I_{\text{net}}^0(\varphi_+, t) - I_{\text{net}}^0(\varphi_-, t)), \tag{D6a}
\end{aligned}$$

$$\begin{aligned}
\mathbf{I}_R^S(t) \cdot \hat{\mathbf{n}}_R = & \frac{1}{2} \times \\
& [I_Q^0(\varphi_+, t) - I_Q^0(\varphi_-, t) - (I_{\text{net}}^0(\varphi_+, t) - I_{\text{net}}^0(\varphi_-, t))]. \tag{D6b}
\end{aligned}$$

Setting the condition $\varphi_{\pm} = \pm\psi_{\text{so}}$ in Eq. (D6) with the help from Eqs. (D2,D3), we then obtain Eq. (77).

* Electronic address: aaharonyaa@gmail.com

† Electronic address: wzhang@mail.ncku.edu.tw

¹ Y. Aharonov and D. Bohm, Phys. Rev. **115**, 485 (1959).

² Y. Aharonov and A. Casher, Phys. Rev. Lett. **53**, 319 (1984).

³ M. Büttiker, Y. Imry, and R. Landauer, Phys. Lett. A **96**, 365 (1983).

⁴ M. Büttiker, Y. Imry, and M. Ya. Azbel, Phys. Rev. A **30**, 1982 (1984).

⁵ Y. Gefen, Y. Imry, and M. Ya. Azbel, Phys. Rev. Lett. **52**, 129 (1984).

⁶ A. G. Aronov, Yu. V. Sharvin, Rev. Mod. Phys. **59**, 755 (1987).

⁷ A. Yacoby, M. Heiblum, V. Umansky, H. Shtrikman, and D. Mahalu, Phys. Rev. Lett. **73**, 3149 (1994).

⁸ A. Yacoby, M. Heiblum, D. Mahalu, and H. Shtrikman,

Phys. Rev. Lett. **74**, 4047 (1995).

⁹ R. Schuster, E. Buks, M. Heiblum, D. Mahalu, V. Umansky, and H. Shtrikman, Nature (London) **385**, 417 (1997).

¹⁰ E. Buks, R. Schuster, M. Heiblum, D. Mahalu, and H. Shtrikman, Nature (London) **391**, 871 (1998).

¹¹ H. Mathur and A. D. Stone, Phys. Rev. Lett. **68**, 2964 (1992).

¹² M. König, A. Tschetschetkin, E. M. Hankiewicz, J. Sinova, V. Hock, V. Daumer, M. Schäfer, C. R. Becker, H. Buhmann, and L. W. Molenkamp, Phys. Rev. Lett. **96**, 076804 (2006).

¹³ T. Bergsten, T. Kobayashi, Y. Sekine, and J. Nitta, Phys. Rev. Lett. **97**, 196803 (2006).

¹⁴ F. Nagasawa, J. Takagi, Y. Kunihashi, M. Kohda, and J. Nitta, Phys. Rev. Lett. **108**, 086801 (2012).

¹⁵ I. Žutić, J. Fabian, and S. Das Sarma, Rev. Mod. Phys.

- 76**, 323 (2004).
- 16 S. Datta and B. Das, *Appl. Phys. Lett.* **56**, 665 (1990).
 - 17 A. Oiwa, Y. Mitsumori, R. Moriya, T. Shupinski, and H. Munekata, *Phys. Rev. Lett.* **88**, 137202 (2002).
 - 18 B. T. Jonker, G. Kioseoglou, A. T. Hanbicki, C. H. Li, and P. E. Thompson, *Nat. Phys.* **3**, 542 (2007).
 - 19 P. LeClair, J. K. Ha, H. J. M. Swagten, J. T. Kohlhepp, C. H. van de Vin, and W. J. M. de Jonge, *Appl. Phys. Lett.* **80**, 625 (2002).
 - 20 T. S. Santos and J. S. Moodera, *Phys. Rev. B* **69**, 241203(R) (2004).
 - 21 M. Gajek, M. Bibes, A. Barthélémy, K. Bouzehouane, S. Fusil, M. Varela, J. Fontcuberta, and A. Fert, *Phys. Rev. B* **72**, 020406(R) (2005).
 - 22 U. Lüders, M. Bibes, K. Bouzehouane, E. Jacquet, J.-P. Contour, S. Fusil, J.-F. Bobo, J. Fontcuberta, A. Barthélémy, and A. Fert, *Appl. Phys. Lett.* **88**, 082505 (2006).
 - 23 G. Schmidt, D. Ferrand, L. W. Molenkamp, A. T. Filip, and B. J. van Wees, *Phys. Rev. B* **62**, R4790 (2000).
 - 24 K. Ando, S. Takahashi, J. Ieda, H. Kurebayashi, T. Trypiniotis, C. H. W. Barnes, S. Maekawa, and E. Saitoh, *Nature Mater.* **10**, 655 (2011).
 - 25 G. Dresselhaus, *Phys. Rev.* **100**, 580 (1955).
 - 26 E. I. Rashba, *Fiz. Tverd. Tela (Leningrad)* **2**, 1224 (1960) [*Sov. Phys. Solid State* **2**, 1109 (1960)]; Y. A. Bychkov and E. I. Rashba, *J. Phys. C* **17**, 6039 (1984).
 - 27 J. Nitta, T. Akazaki, H. Takayanagi, and T. Enoki, *Phys. Rev. Lett.* **78**, 1335 (1997); T. Koga, J. Nitta, T. Akazaki, and H. Takayanagi, *ibid.* **89**, 046801 (2002).
 - 28 T. Koga, Y. Sekine, and J. Nitta, *Phys. Rev. B* **74**, 041302 (2006).
 - 29 J. Nitta, F. E. Meijer, and H. Takayanagi, *Appl. Phys. Lett.* **75**, 695 (1999).
 - 30 D. Frustaglia and K. Richter, *Phys. Rev. B* **69**, 235310 (2004).
 - 31 B. Molnár, F. M. Peeters, and P. Vasilopoulos, *Phys. Rev. B* **69**, 155335 (2004).
 - 32 R. Citro, F. Romeo, and M. Marinaro, *Phys. Rev. B* **74**, 115329 (2006).
 - 33 U. Aeberhard, K. Wakabayashi, and M. Sigrist, *Phys. Rev. B* **72**, 075328 (2005).
 - 34 V. Moldoveanu and B. Tanatar, *Phys. Rev. B* **81**, 035326 (2010).
 - 35 V. M. Ramaglia, V. Cataudella, G. De Filippis, and C. A. Perroni, *Phys. Rev. B* **73**, 155328 (2006).
 - 36 M. J. van Veenhuizen, T. Koga, and J. Nitta, *Phys. Rev. B* **73**, 235315 (2006).
 - 37 P. Földi, O. Kálmán, M. G. Benedict, and F. M. Peeters, *Phys. Rev. B* **73**, 155325 (2006).
 - 38 F. Chi and J. Zheng, *Appl. Phys. Lett.* **92**, 062106 (2008).
 - 39 N. Hatano, R. Shirasaki, and H. Nakamura, *Phys. Rev. A* **75**, 032107 (2007).
 - 40 S.-H. Chen and C.-R. Chang, *Phys. Rev. B* **77**, 045324 (2008).
 - 41 A. Aharony, Y. Tokura, G. Z. Cohen, O. Entin-Wohlman, and S. Katsumoto, *Phys. Rev. B* **84**, 035323 (2011).
 - 42 F. Chi, J.-L. Liu, and L.-L. Sun, *J. Appl. Phys.* **101**, 093704 (2007).
 - 43 F. Chi, X. Yuan, and J. Zheng, *Nanoscale Res. Lett.* **3**, 343 (2008).
 - 44 H.-T. Yin, X.-J. Liu, L.-F. Feng, T.-Q. Lu, and H. Li, *Phys. Lett. A* **374**, 2865 (2010).
 - 45 K.-W. Chen, Y.-H. Su, S.-H. Chen, C.-L. Chen, and C.-R. Chang, *Phys. Rev. B* **88**, 035443 (2013).
 - 46 P. M. Shmakov, A. P. Dmitriev, and V. Yu. Kachorovskii, *Phys. Rev. B* **85**, 075422 (2012); P. M. Shmakov, A. P. Dmitriev, and V. Yu. Kachorovskii, *ibid.* **87**, 235417 (2013).
 - 47 M. Pletyukhov, V. Gritsev, and N. Paudyal, *Phys. Rev. B* **74**, 045301 (2006).
 - 48 A. M. Lobos and A. A. Aligia, *Phys. Rev. Lett.* **100**, 016803 (2008).
 - 49 R. Citro and F. Romeo, *Phys. Rev. B* **73**, 233304 (2006).
 - 50 P. Földi, M. G. Benedict, O. Kálmán, and F. M. Peeters, *Phys. Rev. B* **80**, 165303 (2009).
 - 51 J. Bylander, T. Duty, and P. Delsing, *Nature (London)* **434**, 361 (2005).
 - 52 T. Fujisawa, T. Hayashi, and S. Sasaki, *Rep. Prog. Phys.* **69**, 759 (2006).
 - 53 G. Fève, A. Mahé, J.-M. Berroir, T. Kontos, B. Plaçaïs, D. C. Glattli, A. Cavanna, B. Etienne, Y. Jin, *Science* **316**, 1169 (2007).
 - 54 M. Cini, *Phys. Rev. B* **22**, 5887 (1980).
 - 55 A.-P. Jauho, N. S. Wingreen, and Y. Meir, *Phys. Rev. B* **50**, 5528 (1994).
 - 56 F. B. Anders and A. Schiller, *Phys. Rev. Lett.* **95**, 196801 (2005).
 - 57 J. Maciejko, J. Wang, and H. Guo, *Phys. Rev. B* **74**, 085324 (2006).
 - 58 S. Kurth, G. Stefanucci, C.-O. Almbladh, A. Rubio, and E. K. U. Gross, *Phys. Rev. B* **72**, 035308 (2005).
 - 59 X. Zheng, F. Wang, C. Y. Yam, Y. Mo, and G. H. Chen, *Phys. Rev. B* **75**, 195127 (2007).
 - 60 L. Mühlbacher and E. Rabani, *Phys. Rev. Lett.* **100**, 176403 (2008).
 - 61 T. L. Schmidt, P. Werner, L. Mühlbacher, and A. Komnik, *Phys. Rev. B* **78**, 235110 (2008).
 - 62 J. S. Jin, X. Zheng, and Y. J. Yan, *J. Chem. Phys.* **128**, 234703 (2008).
 - 63 M. W. -Y. Tu and W. -M. Zhang, *Phys. Rev. B* **78**, 235311 (2008); M. W. -Y. Tu, M.-T. Lee, and W. -M. Zhang, *Quantum Inf. Processing (Springer)* **8**, 631 (2009).
 - 64 J. S. Jin, M. W. -Y. Tu, W. -M. Zhang, and Y. J. Yan, *New J. Phys.* **12**, 083013 (2010).
 - 65 D. Segal, A. J. Millis, and D. R. Reichman, *Phys. Rev. B* **82**, 205323 (2010).
 - 66 H. Cruz and D. Luis, *J. Phys.: Conf. Ser.* **99**, 012004 (2008).
 - 67 E. Perfetto, G. Stefanucci, and M. Cini, *Phys. Rev. B* **78**, 155301 (2008).
 - 68 M. W.-Y. Tu, W.-M. Zhang, and J. S. Jin, *Phys. Rev. B* **83**, 115318 (2011); M. W.-Y. Tu, W.-M. Zhang and F. Nori, *ibid.* **86**, 195403 (2012).
 - 69 M. W.-Y. Tu, W.-M. Zhang, J. S. Jin, O. Entin-Wohlman, and A. Aharony, *Phys. Rev. B* **86**, 115453 (2012).
 - 70 Y. Oreg and O. Entin-Wohlman, *Phys. Rev. B* **46**, 2393 (1992).
 - 71 Y. Meir, Y. Gefen, and O. Entin-Wohlman, *Phys. Rev. Lett.* **63**, 798 (1989).
 - 72 A. J. Leggett, S. Chakravarty, A. T. Dorsey, M. P. Fisher, A. Garg, and W. Zwerger, *Rev. Mod. Phys.* **59**, 1 (1987).
 - 73 H. Haug and A.-P. Jauho, in *Quantum Kinetics in Transport and Optics of Semiconductors*, Springer Series in Solid-State Sciences, 2nd ed. (Springer-Verlag, Berlin, 2008), Vol. 123.
 - 74 We define here the orthonormal modes $|+\rangle =$

$(1/\sqrt{2})(d_{1;\hat{n}_1+}^\dagger + d_{2;\hat{n}_2+}^\dagger)$ and $|-\rangle = (1/\sqrt{2})(d_{1;\hat{n}_1+}^\dagger - d_{2;\hat{n}_2+}^\dagger)$. By Eq. (47c), when $\varphi_+ = 2m\pi$, the two electrodes are then bridged by the combination of the original charge basis $|+\rangle$ ($|-\rangle$), leaving the orthogonal one $|-\rangle$ ($|+\rangle$) isolated. The decoupling of one of the combinations of the charge states from the leads for the spinless DQD has led to a distinction in its Hilbert space. Under suitable conditions, decoherence-free states can be dynamically stabilized, as already discussed in a more abstract level in Ref. [75]. This implies that for the DQD AB interferometer with spins for the present concern, the occupation on these modes, $(1/\sqrt{2})(d_{1;\hat{n}_1;+}^\dagger \pm d_{2;\hat{n}_2;+}^\dagger)|0\rangle$, carrying different nonorthogonal spins in different dots, could also be stabilized.

⁷⁵ H. N. Xiong, W. M. Zhang, M. W. Y. Tu and D. Braun, Phys. Rev. A **86**, 032107 (2012).

⁷⁶ The wide-band limit means that there is an infinite number of levels in the reservoir that couple equally strong to the discrete levels in the quantum dot. So every level in the reservoir within this band of infinite width tries to tunnel

to the discrete levels, causing an immediate finite current when the contact begins. This feature of wide-band level-broadening function is also documented.^{55,61} We demonstrate all numerical results in the wide-band limit here for simplicity and for staying connected with our previous work.⁶⁹

⁷⁷ T. Otsuka, E. Abe, Y. Iye, and S. Katsumoto, Phys. Rev. B **79**, 195313 (2009).

⁷⁸ P. Debray, S. M. S. Rahman, J. Wan, R. S. Newrock, M. Cahay, A. T. Ngo, S. E. Ulloa, S. T. Herbert, M. Muhammad, and M. Johnson, Nature Nanotech. **4**, 759 (2009).

⁷⁹ S. Kim, Y. Hashimoto, Y. Iye, and S. Katsumoto, J. Phys. Soc. Jpn. **81**, 054706 (2012).

⁸⁰ T.-M. Chen, M. Pepper, I. Farrer, G. A. C. Jones, and D. A. Ritchie, Phys. Rev. Lett. **109**, 177202 (2012).

⁸¹ T. Hatano, T. Kubo, Y. Tokura, S. Amaha, S. Teraoka, and S. Tarucha, Phys. Rev. Lett. **106**, 076801 (2011).

⁸² J. Verduijn, R. R. Agundez, M. Blaauwboer and S. Rogge, New J. Phys. **15**, 033020 (2013).